INTERNATIONAL ATOMIC ENERGY AGENCY
UNITED NATIONS EDUCATIONAL, SCIENTIFIC AND CULTURAL ORGANIZATION

INTERNATIONAL CENTRE FOR THEORETICAL PHYSICS
34100 TRIESTE (ITALY) - P.O.B. 586 - MIRAMARE - STRADA COSTIERA 11 - TELEPHONE: 2240-1
CABLE: CENTRATOM - TELEX 460392 - 1

SMR/388 - 10

SPRING COLLEGE IN MATERIALS SCIENCE
ON
"CERAMICS AND COMPOSITE MATERIALS"
(17 April - 26 May 1989)

# PLASTICITY AND FRACTURE OF CERAMIC MATERIALS
(Lectures I & II + background material)

Karl KROMP
Institut für Wrkstoffwissenschaft
Max-Planck-Institut für Metallforschung
Seestrasse 92
Stuttgart 7000
Federal Republic of Germany

# Linear - elastic fracture mechanics: (LEFM)

## K - Concept and fracture toughness $K_{Ic}$

brittle materials - ceramics:

linear - elastic at room temperature,

? at high temperature - high loading rates

ceramics - brittle materials:

small defects, grain sized, beyond limit of detection cause catastrophic failure!

dangerousness of defects characterized by "stress intensity" K,

K measure for stress $\sigma$ at the crack front, exceeding that of external load by factors!

$$\sigma \sim \frac{K}{\sqrt{r}}$$

Inglis 1913
Westergaard 1939
Irwin-Williams-Sneddon 1957

r distance from crack front

$$K = \sigma_\infty \sqrt{a}\, Y$$

$\sigma_\infty$ "remote stress", $\sigma_\infty \ll \sigma$ !

a size of defect (crack length)

Y shape factor (correction for finite size)

for the following: only opening mode, $K_I$;
(sliding mode, $K_{II}$, tearing mode, $K_{III}$ are not considered!)

basic for LEFM:

Critical stress intensity $K_c$ → fast fracture

under "certain circumstances":

$K_c$ → "materials constant": $K_{Ic}$

conservative: $K_{Ic} := \min(K_c)$ ⊙

"certain circumstances" for metals and alloys:

ASTM E 399 - 83

guarantees plain strain conditions

→ for ceramics?

ideal brittle at RT - even small specimens (i.g. 3 x 7 x 35 mm³) in plain strain condition

ad $K_{Ic} := \min(K_c)$

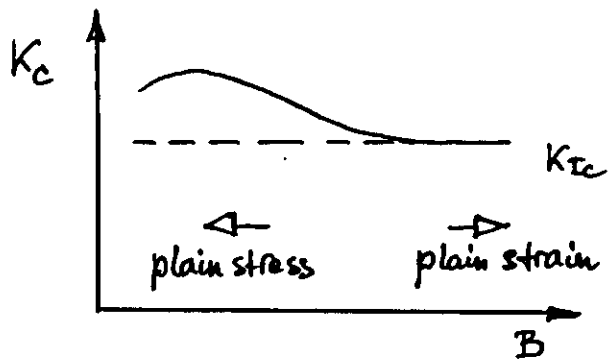


$$K_{Ic} = \sigma_\infty \sqrt{a}\, Y(a/W)$$

plain strain: Constraint in thickness !



Crack growth: Subcritical – critical

Subcritical crack growth:

preceding catastrophic failure by environmental influence → corrosion → finite life time !
higher loading rate → higher strength !

empirical relation,
only justified by experimental results:

$$v = A \cdot K_I^n$$

$$\left(v/v_c = C \cdot (K_I/K_{Ic})^n\right)$$

$v = \dot{a}$ crack growth rate
$n, A$ subcritical crack growth parameters

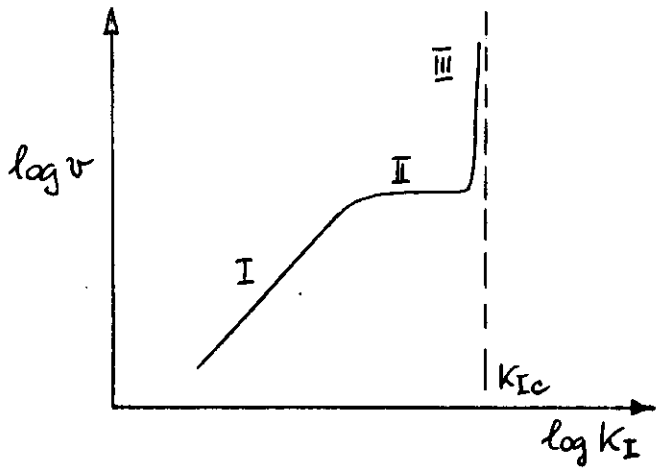


region I: chemical reaction rate

region II: diffusion or flux of corrosive medium

region III: independent of medium, thermal activation (HT only region III)

empirical relation $v = A \cdot K_I^n$ only for region I, in region II $n \ll$, in region III $n \to \infty$

$n_{metals} \sim 4$ $\qquad$ $n_{Ceramics} > 30$

for $K_I \sim \sigma_\infty$ → for ceramics very small load range to observe subcritical crack growth

○ ○

Critical crack growth:

$K_c \to K_{Ic}$, range of $K_{Ic}$, $\dot{a} \gg$



## The problem of $K_{Ic}$ - measurement

basic assumption of LEFM:
Critical stress at a defect of critical length, combined in $K_c$

under "certain circumstances":
. $K_c$ → "materials constant" fracture toughness $K_{Ic}$

standardized for metals and alloys: ASTM E 399-83
→ huge specimens to get plain strain conditions!

seems no problem for ceramics:
ideal brittle, linear elastic → plain strain conditions for very small specimens

new problems:
- difficulty, to produce a starting defect
- dependence of the result on loading rate
  RT: corrosion, HT: weakened second phases

these problems brought about a lot of different methods for measurement and different results!

→ no standardized procedure exists up to now!

# Indentation methods

advantage: only few specimens necessary (one single !)
disadvantage: $K_{Ic}$ - values are only relative values

two main groups:
ICL - and ISB - methods

## ICL "indentation crack length"

procedure: Vickers - indentation of defined load
→ diagonal 2a and crack lengths
l or c are measured

"a" defines Vickers hardness,
combined with crack lengths "l" or "c" → $K_{Ic}$

(Niihara et al., 1982; Anstis et al., 1981)



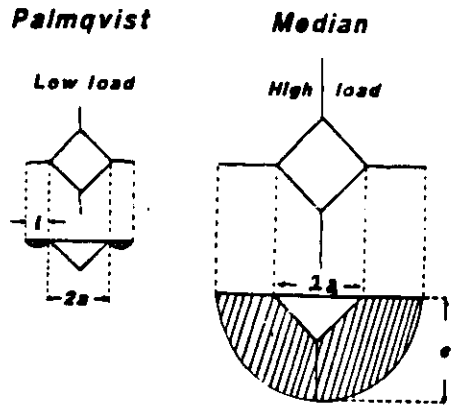


evaluation (Niihara et al., 1982):

for Palmqvist - cracks ($0.25 \leq l/a \leq 2.5$)

$$\left(\frac{K_{Ic}\cdot\phi}{H a^{1/2}}\right)\left(\frac{H}{E\cdot\phi}\right)^{2/5} = 0.129\left(\frac{l}{a}\right)^{-1/2}$$

for Median - cracks ($c/a \geq 2.5$)

$$\left(\frac{K_{Ic}\cdot\phi}{H a^{1/2}}\right)\left(\frac{H}{E\cdot\phi}\right)^{2/5} = 0.129\left(\frac{c}{a}\right)^{-3/2}$$

| | |
|---|---|
| $H$ | Vickers - hardness |
| $a$ | half diagonal of hardness impression |
| $l, c$ | crack lengths |
| $E$ | Young's modulus |
| $\phi$ | constraint factor ($\approx 3$) |

example for results:

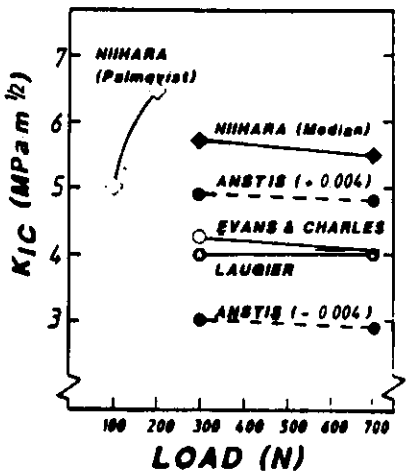


$K_{Ic}$ - values, calculated from indentations by 6 different equations;
$Al_2O_3$, reinforced by 30 Vol% SiC-whiskers
(Ekberg et al., 1989)

This material seems inappropriate for the indentation method, but the diagram demonstrates the relativity of the method!



## ISB "indentation strength in bending"

procedure: indentation on the polished tension-side of a 4-point bending specimen; the hardness-indentation diagonal 2a is measured, strength in bending after indentation.

advantage: crack length needs not to be measured

evaluation (Chantikul et al., 1981):

$$K_{Ic} = \eta_v^R \left(\frac{E}{H}\right)^{1/8} \left(\sigma F^{1/3}\right)^{3/4}$$

| | |
|---|---|
| H | Vickers hardness |
| F | indenter load |
| E | Young's modulus |
| $\sigma$ | fracture stress in 4-point bending |
| $\eta_v^R$ | geometrical constant |

disadvantage: dependence on indenter load and on loading rate in the bending experiment (Lutz et al., 1989).

summarizing at this point:

ICL - method

- easy performance
- one single specimen
- results relative (→ for materials development and quality control)

ISB - method

includes disadvantages of bending experiment

- dependence on loading rate

additionally:

- dependence on indenter load
- dependence on machining of indented surface



bending experiments:

SENB "single-edge-notch in bending"

the most promising candidate for standardization

formulas:

$$K_{Ic} = \sigma_\infty \sqrt{a}\, Y(a/W)$$

$\sigma_\infty$ fracture stress
$a$ length of starting crack (notch)
$Y(a/W)$ correction function (correction for finite size)

fracture stress:

$\sigma_\infty = \sigma_{max}$ below middle loading point in 3-point bending; $\sigma_{max}$ for the unnotched specimen!

$$\sigma_{max} = \frac{3FS}{2BW^2}$$

$F$ fracture load
$S$ span
$W$ width (specimen height)

the correction function $Y$ depends not only on $a/W$, but also on $S/W$!

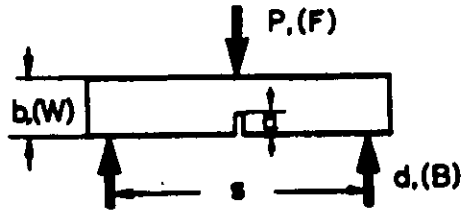


Srawley, 1976:

$a = a/W$

$$Y(a) = \frac{1.99 - a(1-a)(2.15 - 3.93a + 2.7a^2)}{(1+2a)(1-a)^{3/2}}$$

gültig für $0 < a < 1$ und $S/W = 4$

well established at the MPI in Stuttgart,
specimen dimensions $3 \times 7 \times 35\ mm^3$
$S = 30\ mm \rightarrow S/W \triangleq 4$

for 4-point bending experiments:
exchange formulas for $\sigma_{nn} - \sigma_{max}$ and $Y$ !

main problems with SENB:

1) size requirements: ⊙
small influence of specimen thickness by notch-root length

2) influence of fracture-initiating "defect":
restricted to high loading rates
sharp cracks:
- crack length measurements
- dependence of $K_{Ic}$ on crack length
- precracking, SEPB ($K_R$-curve) ⊙

notches:
- independence of notch depth
- dependence on notch width (limit < 100 µm)

O

3) influence of loading rate and temperature
room temperature:
- dependence on loading rate, subcritical crack growth (corrosion)

high temperatures:
- dependence on loading rate
- dependence on temperature at low loading rates

} viscous second phase

O

4) influence of loading equipment
- independence of loaded volume (not for bending strength!)
- dependence on friction effects

ad size requirements:

model material: alumina (Kyocera), grain size 1-3 µm

Carnegie-Mellon Univ. Pittsburgh:

experimental conditions:

W = 12,7 mm (constant)

B = 1,4 ; 2,4 ; 5,3 ; 20 mm

3-point bending, knife edges

S = 28 mm → S/W = 2,2

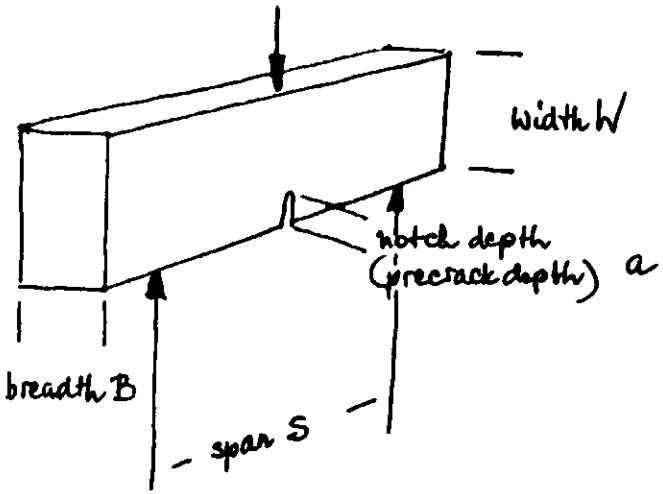




$K_{Ic}$ - measurement: thickness influence 2.

$Al_2O_3$, purity 99.5% (Kyocera)

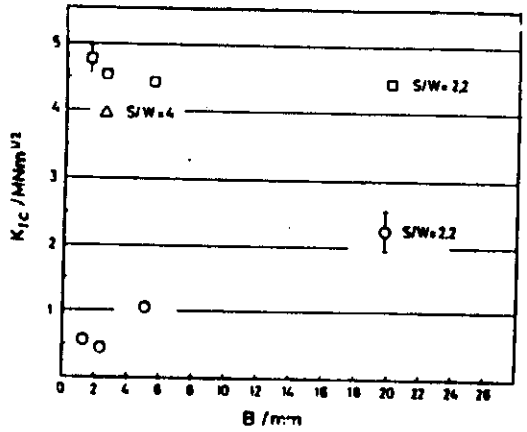


Bild 3: Dickeneinfluß an $Al_2O_3$, Reinheit 99.5%
Kreise: S/W = 2.2, Gurumoorthy et al., 1987;
Quadrate: S/W = 2.2; Dreieck: S/W = 4, Rief und Kromp, 1988.

ad influence of fracture initiating defect:

SEPB "single-edge-precracked beam"

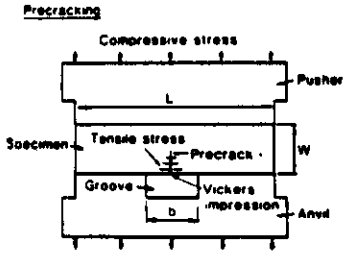


Bild 4a: Schematic of bridge-indentation method. Specimen is sandwiched by a flat pusher and an anvil having a central groove.

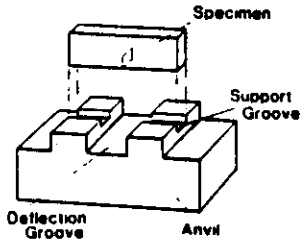


Bild 4b: Perspective view of an anvil. Central groove for the deflection of a specimen surface, a pair of support grooves perpendicular to it, and side cuts to keep the support span from being not more than the specimen length.

procedure: Vickers-indentation on the tension side, loading on an anvil produces sharp crack by "pop in"

(Nose and Fujii, 1988)



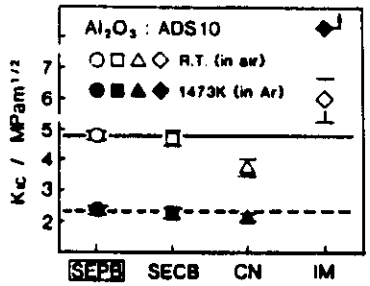


Bild 5: Comparison of $K_c$ values among test methods for $Al_2O_3$ (ADS-11): SEPB (the present method); SECB (single-edge-fatigue-cracked-beam method); CN (chevron-notched-beam method), and IM (indentation-microfracture method).

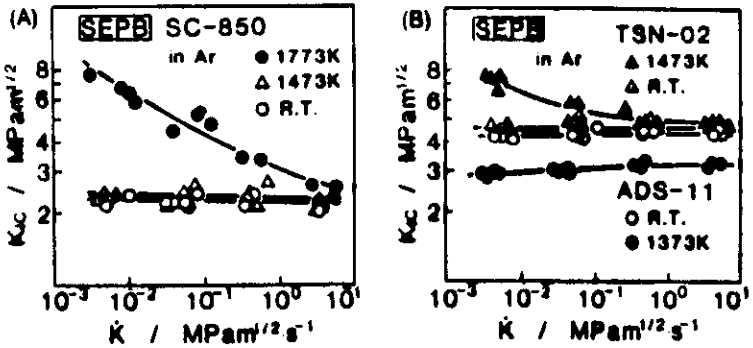


Bild 6: Effect of loading rate of $K_c$ values at room temperature and at elevated temperatures: (A) SiC (SC-850) and (B) $Si_3N_4$ (TSN-02) and $Al_2O_3$ (ADS-11).

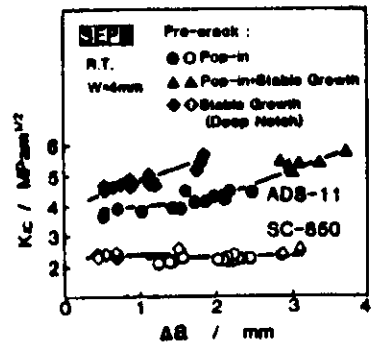


Bild 7 Dependence of $K_c$ on crack extension length for precracks introduced into $Al_2O_3$ (ADS-11) or SiC (SC-850) specimens by either pop-in or stable-crack extension. The nominal grain size of $Al_2O_3$ (ADS-11) is 15 μm.

experiments:

restricted to bending tests;
model material: $Al_2O_3$ + 3 wt% glassy phase,
grain size 10 µm

taken for constant:
- thickness $B \approx 2{,}5$ mm, height $W \approx 7$ mm,
- notch width $\approx 60$ µm, relative notch depth $a/W \approx 0{,}2$

parameters varied:
- testing temperature: 20°C, 1100 °C (→ 5 min)
- loading rate, load controlled ($\dot{\sigma}$ = const.):
  35 MPa/s (≙ 1 mm/min cross-head speed),
  10000 MPa/s
- testing device:
  1) 3-point knife edge support: sapphire ϕ 10 mm, S = 30 mm
  2) 3-point rounded edge support: alumina ϕ 10 mm, ρ = 2,5 mm, S = 30 mm
  3) 4-point rounded edge support ("fixed rollers"): alumina ϕ 10 mm, ρ = 2,5 mm, S = 40/20 mm
  4) 4-point free-roller support: roller ϕ 5 mm, S = 40/20 mm
- surrounding medium: air – vacuum $5 \cdot 10^{-5}$ mbar

seven experiments / test condition;
correction function Y: Srawley 1976 from E 399



Concluding remarks concerning
$K_{Ic}$-measurement by SENB:

Consequences for the establishment of a standardized testing procedure for $K_{Ic}$ as a "materials constant" (note: personal view of the author!):

- perform 3-point bending experiments on knive-edge supports (ϕ 10 mm, radius of edges 2,5 mm)
- simulate starting defects by notches, width < 100 µm
- apply high loading rates to suppress the influence of corrosion at room temperature and that of weakened second phases at high temperatures
- if there arises a dependence on notch width, sharp cracks should be introduced by means of the single-edge-precracked beam
- if a $K_R$-curve effect is observed with sharp cracks, the R-curve should be extrapolated to crack growth $\Delta a = 0$, to obtain the $K_{Ic}$-value

The influence of the loading rate on the results of $K_{Ic}$-measurements at high temperatures announces the limits of the K-concept!

alloys:

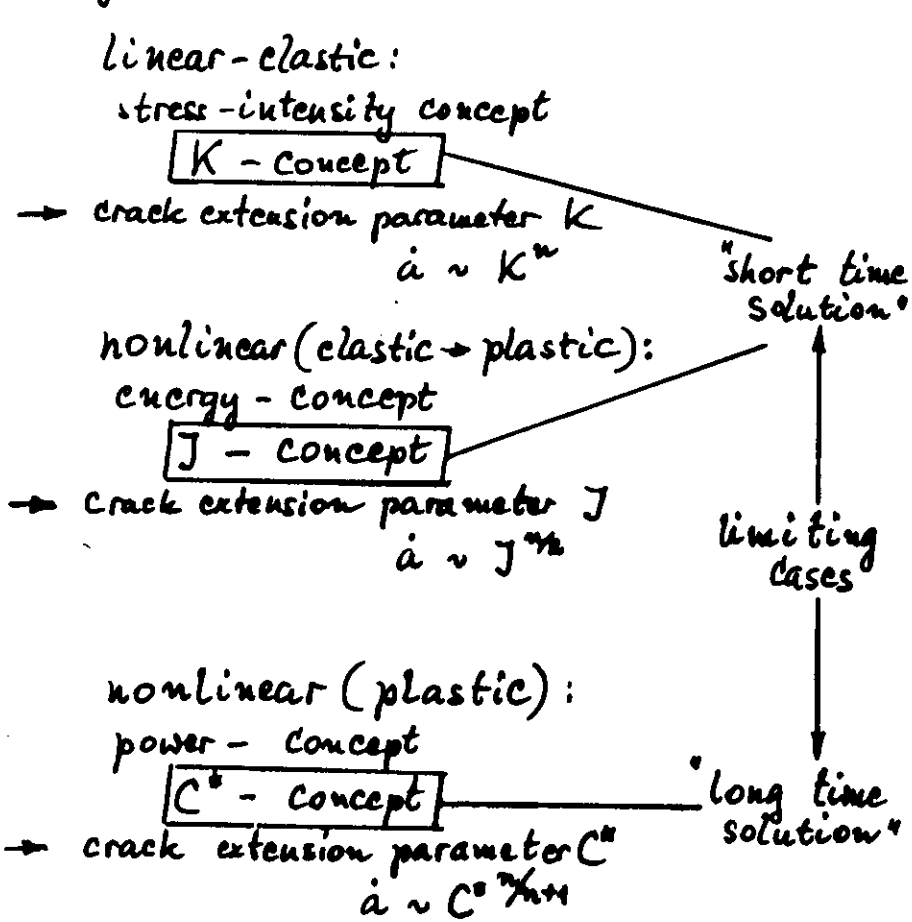


two-phase ceramics ?


Literatur:

1. Anstis, G.R., P. Chanitkul, B.R. Lawn, D.B. Marshall: A critical evaluation of indendation techniques for measuring fracture toughness: I, direct crack measurements; J. Am. Ceram. Soc., 64/9(1981)533-538.

2. Brown, W.F.Jr., J.E. Srawley: Plane strain crack toughness testing of high strength metallic materials; ASTM STP 410(1966)13.

3. Chanitkul, P., G.R. Anstis, B.R. Lawn, D.B. Marshall: A critical evaluation of indendation techniques for measuring fracture toughness: II, strength method; J. Am. Ceram. Soc., 64/9(1981)539-543.

4. Ekberg, I.-L., R. Lundberg, R. Warren, R. Carlsson: Indendation testing of SiC-whisker reinforced $Al_2O_3$ composites; to be published in: Brittle Matrix Composites 2; ed. by A.M. Brandt and I.H. Marshall, Elsevier Appl. Sci. Publ., London-New York.

5. Gurumoorthy, B., H.O.K. Kirchner, F.B. Prinz, G.B. Sinclair: Thickness effects may not do what you think they do; Engng. Fract. Mech. 29/6(1988)637-640.

6. Gurumoorthy, B., K. Kromp, F.B. Prinz, A.C. Bernhauser: Lifetime predictions for a ceramic cutting tool material at high temperatures; J. Mater. Sci. 22(1987)2051-2057.

7. Lutz, E., C. Rief, K. Kromp; erscheint in: Fortschrittsberichte der Deutschen Keramischen Gesellschaft (cfi, ceramic forum international).

8. Niihara, K., R. Morena, D.P.H. Hasselmann: Evaluation of $K_{Ic}$ of brittle solids by the indendation method with low crack-to-indent ratios; J. Mater. Sci. Letters 1(1982)13-16.

9. Nose, T., T. Fujii: Evaluation of fracture toughness for ceramic materials by a single-edge-precracked beam method; J. Am. Ceram. Soc., 71/5(1988)328-333.

10. Rief, C., K. Kromp: erscheint in: Materials Chemistry and Physics, Elsevier Sequoia S.A., Lausanne.

11. Srawley, J.E.: Wide range stress intensity factor expressions for ASTM E 399 standard fracture toughness specimens, Int. J. of Fracture 12(1976)475-476.

12. Steigerwald, E.A.: Crack toughness measurements of high strength steels, review and developments in plane strain fracture toughness testing; ASTM STP 463(1970)102-103

*Int. J. High Technology Ceramics* 4 (1988) 301–317

# 16

# Fracture Toughness Testing

C. Rief & K. Kromp*

Max-Planck-Institut für Metallforschung, Institut für Werkstoffwissenschaften,
D-7000 Stuttgart 1, Seestraße 92, FRG

## 1 INTRODUCTION: FACING A PROBLEM

A basic assumption of linear elastic fracture mechanics is the existence of a critical stress intensity factor, $K_c$, which controls the initiation of fracture. Under certain circumstances this critical value can be regarded as a materials constant, the 'fracture toughness', $K_{Ic}$. The designation 'materials constant' for the fracture toughness means that, for a specific material, the danger posed by a defect in a loaded structure comprising this material is fully characterised by this single parameter. This is normally a conservative approach because $K_{Ic}$ is the $K_c$-value under plane strain conditions, that is the lowest possible $K_c$-value.

It does not seem to be necessary to point out here the high importance of the knowledge of this materials constant for technical purposes. The particular precautions which must be observed while testing in order to guarantee $K_{Ic}$ to be a materials constant are well known for metals and alloys, even in cases where the material's behaviour is far from linear elastic. As a result, the procedure for measuring a $K_{Ic}$-value has been standardised by the ASTM in E399-83. Ceramic materials, at least at low temperatures, can be considered to be linear elastic. This fact seems to free the experimenter from the problem, always connected with metals and alloys, of observing certain requirements in size for the specimens in order to obtain true $K_{Ic}$-values from $K_{Ic}$-tests. Since the grain size of a ceramic material can be neglected compared with the specimen size (which is usually true even for very small test pieces), there should be no problem in obtaining a true 'materials constant' by conducting a $K_{Ic}$-test.

* To whom all correspondence should be addressed



*Int. J. High Technology Ceramics* 0267-3762/88/$03.50 © 1988 Elsevier Science Publishers Ltd, England. Printed in Great Britain

Despite these convenient presumptions, $K_{Ic}$-measurements on ceramic materials, even at room temperature, have produced many different results and shown up many problems. It seems necessary to standardise one or even several special procedures in order to get true $K_{Ic}$-type materials constants for ceramics. To the authors' knowledge, the discussion of this problem has been initiated in the US (Quinn, G., 1987, pers. comm.) and also in Europe in Britain, France and Italy. In the FRG, the German Institute for Industrial Standardisation (DIN) held a meeting in February 1988, which was attended by one of the authors. It was announced that DIN would start its activities in this particular field in June 1988.

The aim of the present work is to point out the main problems arising in $K_{Ic}$-testing with ceramic materials and to contribute the results of some specific experiments to defining a standard procedure for $K_{Ic}$-testing. The present work is confined to bend tests, because in the authors' opinion these seem to be the most promising candidates for a standardised testing procedure.

## 2 STATE OF THE ART

Several problems in $K_{Ic}$-bend testing with ceramic materials are already well documented. In this section these problems will be discussed first, to show the relevance of the authors' own experiments.

### 2.1 Size requirements: influence of specimen thickness

As already mentioned, ceramic materials can be regarded as ideally brittle and thus linear elastic, at least at room temperature. There should be no special specimen size requirements, especially for thickness, because unlike for metals and alloys, plane strain conditions always exist. For example, it was shown that for an alumina containing a glassy phase at room temperature it is not necessary at room temperature to comply exactly with the ASTM E399 size requirements for bending tests, because a variation in specimen size has almost no influence on the $K_{Ic}$-values (Pabst, 1972). The same author showed that a variation in the loaded volume up to a factor of 40 had no influence on the results.

A slight influence of thickness could occur when notches are used to initiate fracture instead of sharp natural cracks. This influence results from inhomogeneities in the notch root originating from the combined effect of the polycrystalline structure and the diamond grit of a saw blade. There appears to be a dependence on the 'surface structure' of the notch root similar to the dependence of the bend strength on the surface finish. An



attempt was made to modify Weibull statistics to account for the defects along the length of a notch root (Tradinik *et al.*, 1982). This statistical investigation showed that the influence of thickness on $K_{Ic}$ was very small.

Summarising at this point, it appears that variations in specimen size, especially in thickness, seem to have only a small influence on $K_{Ic}$-test results. Therefore, in the present investigation, the size and thickness of the specimens were kept constant.

### 2.2 Influence of different fracture-initiating defects

In $K_{Ic}$-testing, critical fracture starts at an artificial 'defect'. The surface finish of the specimen, which plays a most important role in bend tests, has no influence on the results in $K_{Ic}$-testing. The artificial initiating defect can be a sharp crack or a notch. The following statements concerning sharp cracks or notches for a starting defect are valid only for $K_{Ic}$-testing at a high loading rate; for low loading rates there is an additional loading rate influence (see Section 2.3).

Sharp cracks can be introduced into the specimen by indentation, or in controlled growth experiments (Chantikul *et al.*, 1981; Wieninger *et al.*, 1986). When a sharp crack is used as the initiating defect for a $K_{Ic}$-test, two problems arise:

crack length measurement;
a dependence of $K_{Ic}$ on crack length ($K_R$-curve effect).

Different methods of crack length measurement have been proposed, such as direct observation during controlled loading, a side illumination technique, or the identification of the starting crack length on the fracture surface after the $K_{Ic}$-test. These methods produce equivalent results (Wieninger *et al.*, 1986).

For specific materials such as coarse-grained alumina, zirconia, and for alumina with a glassy phase (the latter only at high temperatures), a dependence of the $K_{Ic}$-values on the lengths of the natural cracks as starting defects has been found (Wieninger *et al.*, 1986, 1987). The symbols (●) in Figs 1 and 2 demonstrate this strong dependence.

Using notches for the starting defects, $K_{Ic}$ does not depend on the depth of the notches, at least at high loading rates (symbols (○) in Figs 1 and 2). With notches, another problem arises: the dependence of $K_{Ic}$ on the notch width. It was found that, in both 3- and 4-point bending, in the limit of notch width $\rightarrow 0$ (equivalent to the radius of curvature in the notch root $\rightarrow 0$), a minimum value of $K_{Ic}$ may be reached (Pabst, 1972; Popp, 1981). In Fig. 3 this is shown for $K_{Ic}$-measurements with alumina at room temperature (Bretfeld *et al.*, 1981). The symbols (○) are the mean values of 10 measurements, performed

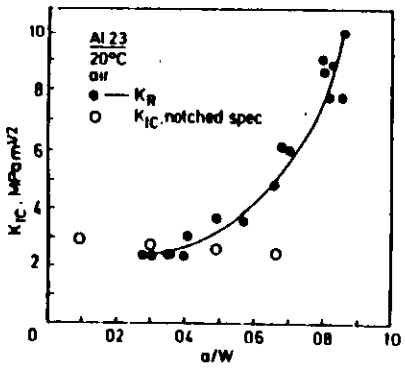


**Fig. 1.** $K_R$-curve for coarse-grained alumina at room temperature; $K_{IC}$-test at a loading rate of 1000 N/s. ○ = notched specimens (notch width 60 μm); ● = specimens with natural sharp cracks (Wieninger *et al.*, 1986).

at the Max-Planck-Institut, Stuttgart (the material is the same as that used for the present investigation). Figure 4 demonstrates this behaviour for silicon-infiltrated SiC at room temperature (Popp, 1981). Figures 1 and 2 support this point of view. The crack width necessary to get the minimum $K_R$-level for the materials discussed above was $< 100\,\mu m$.

Summarising this section it may be stated that:

> with natural, sharp cracks for the starting defect for certain ceramic materials at low or high temperatures, a strong dependence on the depth of the crack may appear;
> with notches for the starting defect, the dependence on the depth of the defect vanishes, but a dependence on the width of the notch arises;

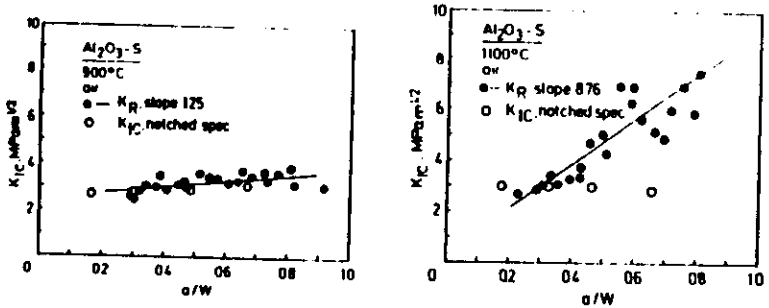


**Fig. 2.** $K_R$-curves for alumina with glassy phase: (a) at 900 °C, (b) at 1100 °C. $K_{IC}$-test at a loading rate of 1000 N/s. ○ = notched specimens (notch width 60 μm); ● = specimens with natural sharp cracks (Wieninger *et al.*, 1987).



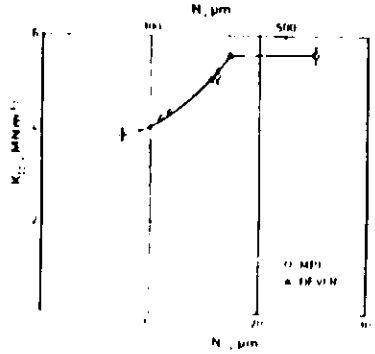


**Fig. 3.** Dependence of $K_R$ on notch width: alumina at room temperature, 4-point bending, cross-head speed 0.5 mm/min; ▽ = notch depth to height ratio 0.2; △ = notch depth to height ratio 0.5 (Bretfeld *et al.*, 1981).

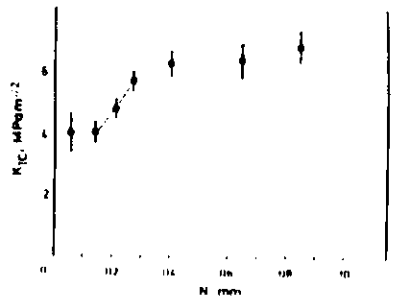


**Fig. 4.** Dependence of $K_R$ on notch width: silicon-infiltrated SiC at room temperature, 4-point bending, cross-head speed 0.05 mm/min; ◆ = notch depth to height ratio 0.2 (Popp, 1981).

> with notch widths below a certain limit ($< 100\,\mu m$), both the dependence on depth and on width of the starting defect seem to vanish.

In the present investigation, therefore, starting defect notches with widths of about 60 μm were used. However, it should be noted that these statements on notch width cannot necessarily be generalised for all materials, but the principles probably apply to most of them.

### 2.3 Influence of loading rate and temperature

At room temperature in air, a slight increase of $K_{IC}$-values with loading rate was found for alumina materials (Kromp & Pabst, 1981; Bretfeld *et al.*, 1981). Figure 5 shows this loading-rate dependence for pure alumina and for the same alumina with a glassy phase used in the present investigation. The reason for this dependence is subcritical crack growth in a corrosive environment, such as air, taking place prior to fast fracture at low loading rates. This subcritical crack growth is usually not accounted for when calculating $K_{IC}$.

At high temperatures for two-phase materials (alumina with a glassy phase, silicon-infiltrated SiC, and $Si_3N_4$ with sintering aids) in certain temperature ranges where the second phase changes to a viscous or plastic state, a strong dependence on loading rate appears. This dependence is demonstrated in Fig. 6 for alumina with a glassy phase at 900 °C. For comparison, in the same figure the pure alumina exhibits only a slight dependence, similar to that at room temperature.

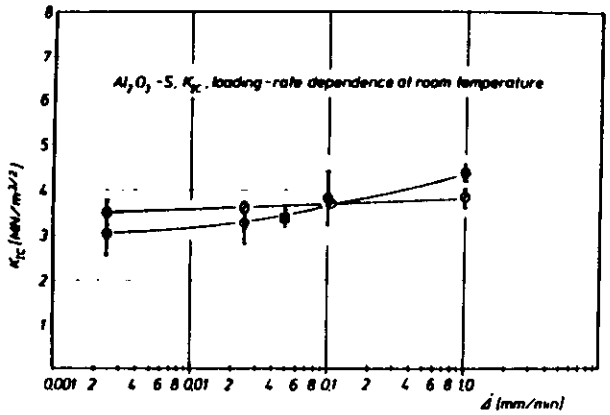


Fig. 5. Dependence of $K_{IC}$ on cross-head speed at room temperature. $\frac{\Delta}{\Delta}$ = pure alumina; $\frac{\Delta}{\nabla}$ = alumina with glassy phase, 3-point bending, notch depth to height ratio 0.2; $\frac{\Phi}{\Phi}$ = $K_{IC}$ literature (Kromp & Pabst, 1981).

On the other hand, the state of the second phase gives rise to a strong temperature-dependence on $K_{IC}$ in the low loading rate range. Both the loading rate and the temperature-dependence are demonstrated in Fig. 7 for silicon-infiltrated SiC. Summarising this section:

- at low temperatures, subcritical crack growth and thus corrosion gives rise to a dependence on loading rate;

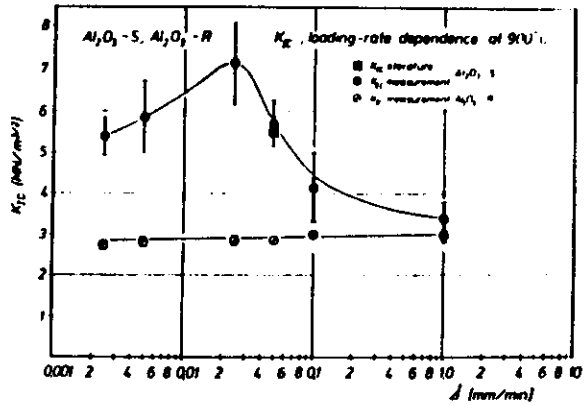


Fig. 6. Dependence of $K_{IC}$ on cross-head speed at 900 °C. $\frac{\Delta}{\Delta}$ = pure alumina; $\frac{\Phi}{\Phi}$ = alumina with glassy phase, 3-point bending, notch to height ratio 0.2 (Kromp & Pabst, 1981).



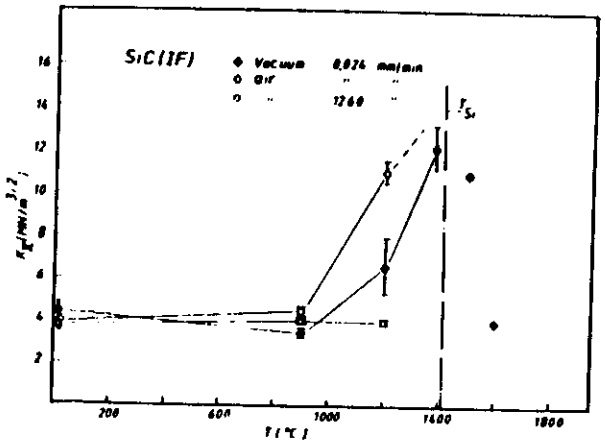


Fig. 7. Dependence of $K_{IC}$ on cross-head speed and on temperature for silicon-infiltrated SiC; 3-point bending, notch depth to height ratio 0.2 (Popp, 1982).

- at high temperatures, the change in the viscous or plastic state of a second phase gives rise to a strong dependence on temperature and loading rate;

these dependences should vanish if very high loading rates are applied. This point is the subject of the present investigation.

### 2.4 Influence of loading equipment

In tests of the bend strength in 3- or 4-point bending, the size of the loaded volume has a strong influence on the result. Also, there is an influence resulting from loading on knife edges, round-ground edges ('fixed rollers'), or free-moving rollers.

For $K_{IC}$-testing, to the authors' knowledge, there is little information on this dependence. In general, any effect should not be as marked as in bend strength tests; for example, there should be no dependence on loaded volume. The only effect could be a result of friction from using fixed-edge supports instead of roller supports. This effect is also a subject of the present investigation.

## 3 EXPERIMENTS

The aim of the present investigation is to establish experimental conditions for $K_{IC}$-testing to obtain a true 'materials constant'. As already indicated,

the investigation is restricted to the bend test, which is a promising candidate for such a test procedure. Of the group of parameters that influence the test results, some are held constant and the more important ones are varied.

Taken as constant are:

- the specimen thickness $B$ and height $W$ (Section 2.1);
- the notch width and depth (Section 2.2).

The parameters which are varied are:

- the testing temperature (Section 2.3);
- the loading rate (Section 2.3);
- the testing device (Section 2.4).

### 3.1 Experimental equipment

The tests were performed in a vacuum vessel connected to a hydropulsing system, to guarantee quick response at high loading rates. The high temperature was achieved by induction heating using a $MoSi_2$ susceptor tube. The susceptor was insulated from the water-cooled induction coil by a thin-walled alumina tube. The vacuum vessel and the 4-point loading jig (see below) are shown in Fig. 8.

The experiments were performed under load-control (stress rate

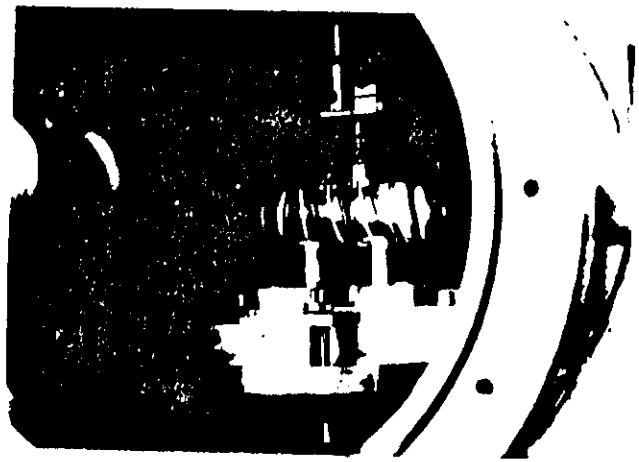

Fig. 8. Vacuum vessel with 4-point bending device with rounded-edge supports (radius 2·5 mm) at 1100 °C in air.



$\dot{\sigma}$ = constant). The load-time relation was registered on a transient recording system. Four different loading systems were tested:

- a 3-point knife-edge support; sapphire single-crystal rods with diameter of 10 mm, machined to knife edges; span $S = 30$ mm;
- a 3-point rounded-edge support; the radius of curvature of the edges was 2·5 mm, machined from alumina rods with diameter of 10 mm; span $S = 30$ mm;
- a 4-point rounded-edge support ('fixed-roller support'); the radius of curvature of the edges was 2·5 mm, machined from alumina rods with diameter of 10 mm; outer span $S = 40$ mm, inner span $S - 2c = 20$ mm (see Fig. 8);
- a 4-point free-roller support; roller diameter = 5 mm; outer span $S = 40$ mm, inner span $S - 2c = 20$ mm.

The complete experimental system included: vacuum vessel, hydropulsing system, induction heating system, temperature- and load-control units, transient recorder, x–y recorder and computer.

### 3.2 Experimental conditions

An alumina with 3% wt glassy phase, a mean grain size of 10 $\mu$m, Young's modulus 360 GPa and a density of $3{\cdot}82 \times 10^3$ kg/m$^3$ were used as model material for the experiments.

The specimens had lengths of 68 or 34 mm, a thickness $B = 2{\cdot}55 \pm 0{\cdot}27$ mm and a height $W = 7{\cdot}0 \pm 0{\cdot}25$ mm. They were notched to a notch length to height ratio $a/W = 0{\cdot}17 \pm 0{\cdot}03$ by means of a diamond-covered copper blade with a thickness of 50 $\mu$m, resulting in a notch width of about 60 $\mu$m.

Experiments were performed at room temperature and at 1100 °C. The inertia of the inductive heating system being very low, the level of 1100 °C was reached in 5 min.

A cross-head speed of the order 1 mm/min is usually chosen for technical convenience in $K_{IC}$-testing. With displacement and span for the individual specimen size and material used in this investigation, a corresponding stress rate of $\dot{\sigma} = 35$ MPa/s† was calculated. This relatively low stress rate was applied in the present experiments in order to allow a comparison of the results with those from other investigations.

† The calculated stressing rate is based on the rate of application of load to a solid beam showing the same flexural characteristics as the notched beam in question, and is thus a purely nominal rate unrelated to the acutal stress field in the specimen.

It should be emphasised here that an experiment performed at a constant cross-head speed is an uncontrolled experiment, for neither load nor displacement are controlled.

Additionally, a very high stress rate of $\dot{\sigma} = 10000$ MPa/s was chosen to rule out all effects that arise at the low stress rates (see Section 4). The stress rates were individually calculated for each specimen because the dimensions of the specimens varied by a certain amount as stated above.

Seven experiments were performed for each test condition; the mean and maximum deviations of these groups of seven experiments are presented. For the calculation of the $K_{IC}$-values, three different geometric correction functions $Y(a:W)$ were employed: Srawley (1976), Steigerwald (1970) and Brown & Srawley (1966). The results were almost identical; the first (Srawley, 1976) was generally used for the further calculations.

## 4 EXPERIMENTAL RESULTS AND DISCUSSION

### 4.1 Influence of the testing device on $K_{IC}$-results

At first, experiments with the four different loading jigs were performed at 20 and 1100°C. To attempt to rule out the expected influence of corrosion at 20°C and the influence of the second phase at 1100°C, the high stress rate of $10^4$ MPa/s was applied in both sets of experiments. Figure 9 shows the results. It is obvious that the levels of $K_{IC}$-values are different for 20°C ($K_{IC} = 3{\cdot}81$) and 1100°C ($K_{IC} = 2{\cdot}97$). This decrease with increasing temperature was expected.

The 3-point knife edge, and the 3- and 4-point rounded-edge support systems gave nearly identical results at room temperature. Only the 4-point free-roller system led to a 5% lower value (Fig. 9). This result could also be expected, because fixed-support systems give rise to friction between test specimen and support, and thus to higher sustained loads prior to fast fracture.

Unfortunately, a free-roller support for high temperatures was not available. Therefore, this friction effect could not be demonstrated at 1100°C. Only the fixed systems could be tested at the high temperature, but the 4-point rounded-edge support system obviously produced higher friction than the 3-point systems (Fig. 9).

Additionally, at the high temperature the influence of a misalignment was tested for the 4-point rounded-edge support. One of the inner support edges



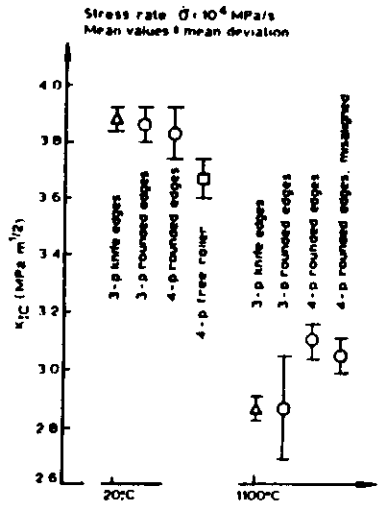


Fig. 9. Influence of the specific testing device on $K_{IC}$-results. Stress rate: 10000 MPa s, mean values ± mean deviation.

was turned by 20° in the plane of the specimen. The influence of such a misalignment was very small (Fig. 9).

Summarising this section:

— 3- or 4-point testing devices give equivalent results, which would not be true for bend strength measurements;
friction effects have an influence on the results: systems with fixed supports show higher values than systems with free rollers. At high temperatures for the systems with fixed supports, the 4-point systems show higher values than the 3-point systems.

It should be mentioned here that the free-roller system was not free to pivot about an axis parallel to the length of the specimen—this point needs to be investigated separately. If the specimens are well machined, i.e. the surfaces are plane and parallel, then in the authors' opinion the absence of ability to pivot should have little influence on the result.

All these deviations are less than 10%. If one recognises the scatter of the measurements for the particular testing jigs (the maximum deviations for the particular devices are shown in Fig. 10), it could be stated that for $K_{IC}$-testing, the influence of a specific loading device on the results is not significant.

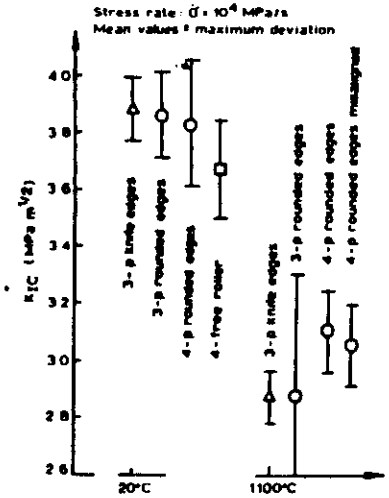


**Fig. 10.** Influence of the specific testing device on $K_{IC}$-results. Stress rate: 10000 MPa/s, mean values ± maximum deviation.

Concluding this section, it is found that the 3-point knife-edge support system shows the smallest scatter, especially at the high temperature. It may well be that this system is the best for defining the test conditions (see Fig. 10).

### 4.2 Influence of loading rate and temperature on $K_{IC}$-results

As already discussed in Section 2.3, the loading rate and the testing temperature mutually influence the results of $K_{IC}$-testing. The following measurements were all performed with the 3-point rounded-edge supports. To clarify the influence of water-vapour corrosion, measurements in air were compared with measurements in a vacuum of $5 \times 10^{-3}$ Pa.

At the high stress rate of $10^4$ MPa/s, the results of the measurements in air and in vacuum at 20°C were identical. At 1100°C, the result for the vacuum measurement was at a slightly higher level compared to the test in air, but the scatter bands of both tests overlapped (Fig. 11). Both vacuum results at the very high stress rate were about the same as the measurements in air already shown in Fig. 9.

The low stress rate of $\dot{\sigma} = 35$ MPa/s, corresponding to the loading rate commonly used, gave a variety of results. For this low rate, the result in the corrosive environment at room temperature was distinctly lower (15% less),



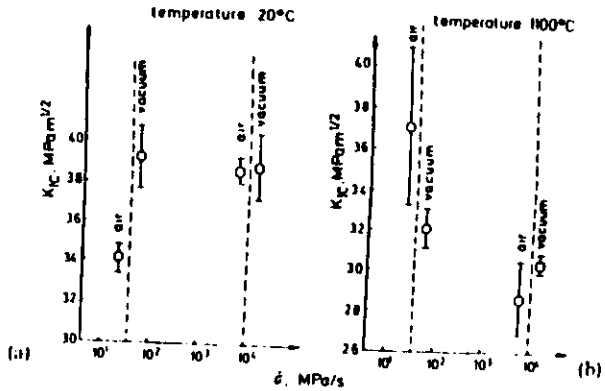


**Fig. 11.** Influence of loading rate on $K_{IC}$-results (stress rates of 35 and 10000 MPa s$^{-1}$) in air and in vacuum (mean values ± mean deviation): (a) at room temperature, (b) at 1100 °C.

while the value in vacuum was at about the same level as the high stress rate result (Fig. 11). Only subcritical crack growth prior to fast fracture could be the cause for this deviation in air. From the fracture surfaces, this fact could hardly be detected. In general, the fracture surfaces for the low stress rate in an air environment appear more intergranular than those of the specimens broken at the high stress rate (compare Figs 12(a) and (b)).

At 1100°C, the results for the low stress rate were higher than those for the high stress rate (Fig. 11): this fact was noted previously (see Fig. 6). Subcritical crack growth, which at these temperatures can only result from thermally activated processes, does not play an important role. This high level of $K_{IC}$-values at the low stress rate may result from the blunting of microcracks by the viscous flow of the glassy phase. Viscous flow is energy-absorbing and results in a higher $K_{IC}$-level. This can be observed directly on the fracture surfaces; an example is given in Fig. 13. The glassy phase covers the grains and moves to triple junctions, thus blunting microcracks, which start predominantly from these positions (see especially Fig. 13(b), at the lower left of the picture).

To summarise this section:

- at low loading rates and temperatures, corrosive subcritical crack growth takes place and reduces the level of the $K_{IC}$-values;
- at low loading rates and high temperatures, energy-absorbing effects caused by the low-viscosity state of the second phase occur and thus raise the $K_{IC}$-values;
- at very high loading rates, these effects do not occur.

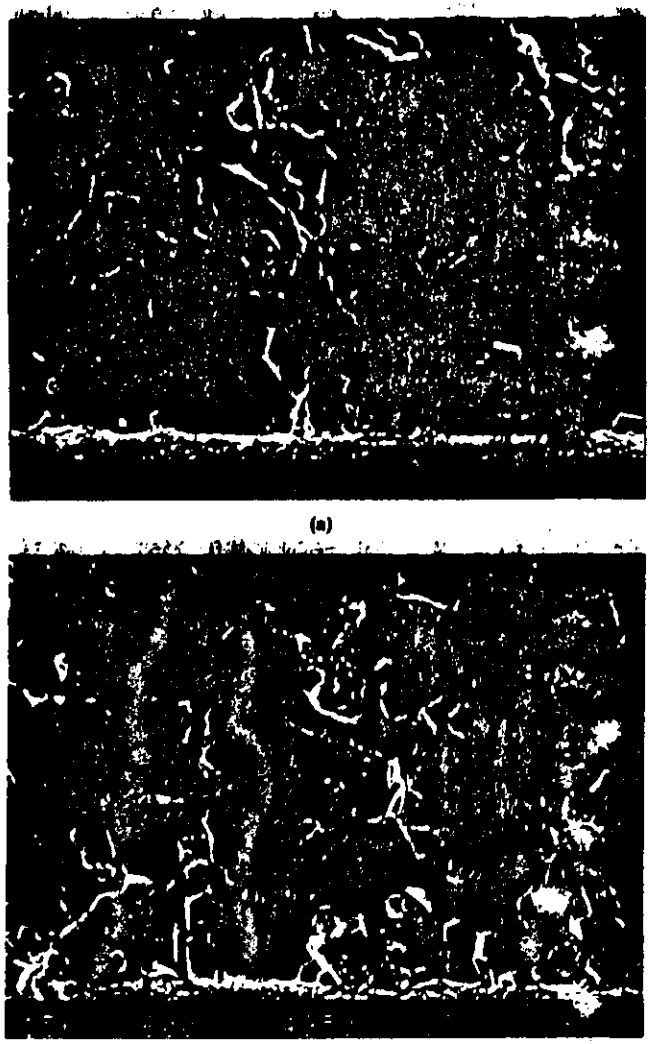

(a)

(b)

Fig. 12. Fracture surfaces at different stress rates (a) 35 MPa/s, and (b) 10000 MPa/s; room temperature in air. The notch root appears at the foot of the images.



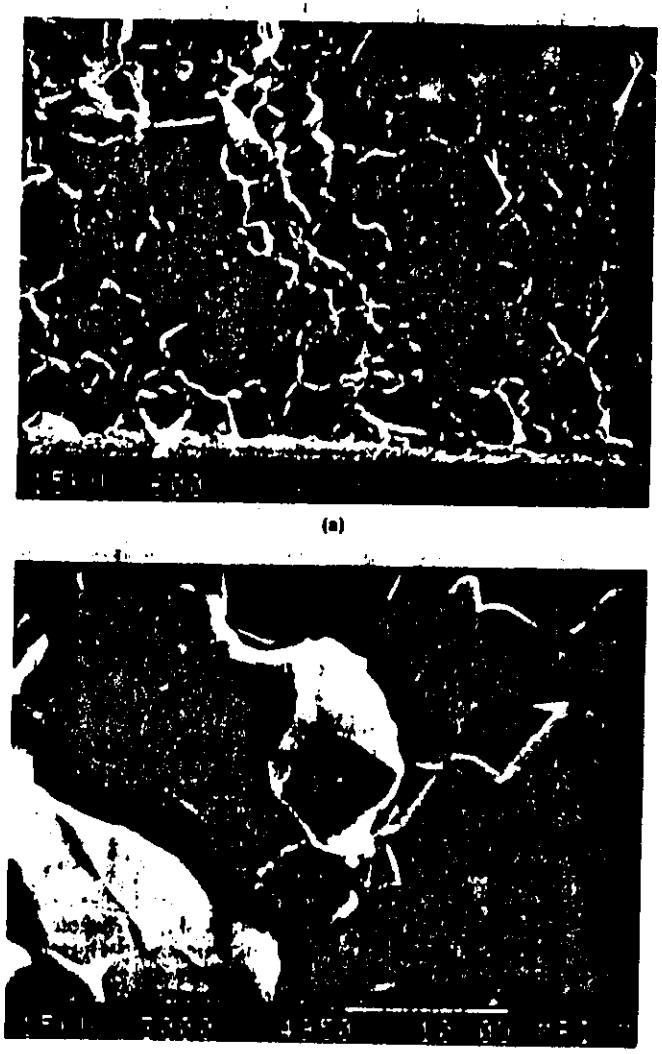

(a)

(b)

Fig. 13. Fracture surface: stress rate 35 MPa/s at 1100°C in vacuum. The notch root appears at the foot of the images. Image (b) shows detail from image (a).

## 5 SUMMARY AND CONCLUDING REMARKS

The bending method is a promising candidate for a standard $K_{IC}$-testing procedure. First, the influences of the specimen dimensions, the fracture-initiating defect, the loading rate, the temperature and the use of specific loading fixtures were discussed. Then, experiments were presented using an alumina with 3% wt glassy phase as a model material to clarify the influence of a specific loading jig: i.e. 3-point bending with knife-edge supports; 3- and 4-point bending with rounded-edge supports ('fixed-roller supports'); and 4-point bending with free-roller supports. Additionally, the influence of two extremely different loading rates (stress rates of 35 MPa/s and 10 000 MPa/s) and two different temperatures (20 and 1100°C) was elucidated by the experimental results.

The following conclusions for the establishment of a testing procedure for the measurement of $K_{IC}$ as a 'materials constant' can be drawn, provided that a notch of width $< 100\,\mu m$ is used for the starting defect:

with different loading fixtures, the results differ by only a few per cent; therefore a 3-point bending system with knife-edge supports would be suitable, because it is easier to use compared with 4-point free-roller systems, especially at high temperatures;

—the commonly applied loading rates (cross-head speeds) in the range of 1 mm/min are to be avoided, because they produce conditions where the influences of corrosion at low temperatures and of a second phase at high temperatures is greatest:

—very high loading rates should be applied, because with these the influences of corrosion and second phases vanish.

## REFERENCES

Bretfeld, H., Kleinlein, F. W., Munz, D., Pabst, R. F. & Richter, H. (1981). Ermittlung des Bruchwiderstandes an Oxidkeramik und Hartmetallen mit verschiedenen Methoden. *Z. Werkstofftech.*, **12**, 167–74.

Brown, W. F., Jr & Srawley, J. E. (1966). Plane strain crack toughness testing of high strength metallic materials, ASTM STP 410, p. 13.

Chantikul, P., Anstis, G. R., Lawn, B. R. & Marshall, D. B. (1981). A critical evaluation of indentation techniques for measuring fracture toughness: II, strength method, *J. Am. Ceram. Soc.*, **64**(9), 539–43.

Kromp, K. & Pabst, R. F. (1981). High-temperature J-integral measurements and micromechanisms at crack tip of ceramic materials, *Metal Sci.*, **15**, 125–9.

Pabst, R. F. (1972). PhD thesis, Stuttgart University, FRG.

Popp, G. (1982). PhD thesis, Stuttgart University, FRG.



Srawley, J. E. (1976). Wide range stress intensity factor expressions for ASTM E399 standard fracture toughness specimens, *Int. J. of Fracture*, **12**, 475–6.

Steigerwald, E. A. (1970). Crack toughness measurements of high strength steels, review and developments in plane strain fracture toughness testing, ASTM STP 463, pp. 102–3.

Tradinik, W., Popp, G. & Pabst, R. F. (1982). Untersuchungen zur Volumenabhängigkeit von $K_{IC}$-Daten mit Hilfe einer modifizierten Weibullstatistik, *Z. Werkstofftech.*, **13**, 254–8.

Wieninger, H., Kromp, K. & Pabst, R. F. (1986). Crack resistance curves of alumina and zirconia at room temperature, *J. Mater. Sci.*, **21**, 411–18.

Wieninger, H., Kromp, K. & Pabst, R. F. (1987). Crack resistance curves of alumina at high temperatures, *J. Mater. Sci.*, **22**, 1352–8.

JOURNAL OF MATERIALS SCIENCE 21 (1986) 411-418

# Crack resistance curves of alumina and zirconia at room temperature

H. WIENINGER, K. KROMP*
*Institut für Festkörperphysik, University of Vienna, A-1090 Vienna, Austria*
R. F. PABST
*Max-Planck-Institut für Metallforschung, Seestrasse 92, 7000 Stuttgart 1, Federal Republic of Germany*

Ceramic three-point bend specimens were pre-cracked in a displacement-controlled test in air at room temperature to form sharp cracks of different lengths. Critical stress intensity factors ($K_{Ic}$) were then measured as a function of sharp crack length in a fast-fracture, load-controlled test. Crack resistance curves ($K_{Ic}$ against crack length) were determined for three commercially pure aluminas of different grain size, a debased alumina containing a glassy phase, and a partially stabilized zirconia (PSZ) material. The crack resistance curves proved to be flat for the finer-grained and the debased alumina. A steeply rising crack resistance curve was, however, observed for a pure coarse-grained alumina material which is explained by friction effects of the cracked microstructure behind the measured crack front. The effect is influenced by the test procedure itself. Though crack branching takes place the crack resistance curve of PSZ is completely flat, which is attributed to fast fracture testing where only the most dangerous flaw is activated.

## 1. Introduction

Ceramic materials are normally completely brittle at room temperature. The brittleness implies that linear elastic fracture mechanics is best suited for fracture toughness measurements and subcritical crack extension characterization. It may be assumed that the fracture toughness value turns out to be a material constant independent of crack length.

In contradiction to these presumptions it was found in an earlier paper [1] that fracture toughness data measured with sharp cracks showed a strong dependence on crack length, in which the fracture toughness or crack resistance increases with increasing crack length.

The load–displacement records of the experiments leading to this dependency were performed in a more or less controlled manner, and showed increasingly non-linear behaviour with increasing sharp, natural crack lengths [2].

In analogy with plasticity reactions with metallic materials the effect was first explained by a "process zone" of microcracking *ahead* of the actual crack tip, the size of the microcracks being typically of the order of the structural element (i.e. the grain size). The rising crack resistance curve was then explained by an enlargement of this "process zone" with increasing crack length, in complete analogy with the increase in the size of the plastic zone found in metallic materials.

However, as a "process zone" could not be detected [2] it was then alternatively argued [1, 2] that friction effects or adhesive forces at the crack surfaces *behind* the actual crack tip cause the unusual behaviour. These arguments were supported by measurements with narrow notches which guarantee traction-free crack surfaces. It could be proved that crack resistance curves measured with narrow notches are completely flat [1] (Fig. 1). Meanwhile similar behaviour was found by other authors [3–6] and a broad discussion has developed about the pre-conditions and the nature of this strange phenomenon.

The existence or non-existence of a rising crack resistance curve has very important practical consequences: the question is whether a single fracture toughness parameter is sufficient to characterize catastrophic failure or if a crack resistance curve is necessary.

As mentioned above, the fracture toughness data (as a function of crack length) were evaluated from more or less subcritical, displacement-controlled tests which can cause crack branching and microcrack formation. If fracture toughness should characterize the catastrophic failure in a linear elastic test, then rapid, load-controlled experiments should be performed, as in the present work. Nevertheless, sharp cracks of distinct lengths have to be introduced by a displacement-controlled subcritical test procedure.

For the experiments a variety of materials were chosen with different tendencies towards secondary crack formation and microcracking.

## 2. Experimental procedure

The $K_I$ curves were determined as listed below.

### 2.1. The precracking process

Three-point bend specimens 7 mm × 2.5 mm × 40 mm in size (span width 30 mm) were notched to a normalized notch depth of 0.2 and then pre-cracked to the desired natural crack length in a displacement-controlled test in air at room temperature. The displacement rate of 1 $\mu$m min$^{-1}$ promotes crack branching and microcracking. After the desired sharp crack length was reached the specimens were unloaded. The displacement-controlled test was made possible by using an extremely stiff bending device with SiC supports together with a stiff testing machine of very low compliance $C_m = 0.0109 \pm 0.0003\,\mu m\,N^{-1}$. The displacement was directly measured and controlled by a linear voltage differential transformer in contact with the lower specimen surface.

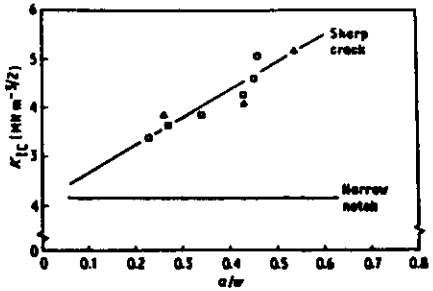


*Figure 1* $K_R$ values for $Al_2O_3$, measured with sharp cracked and notched specimens [1].

### 2.2. Crack length measurement

As there is no macroscopic blunting effect with ceramic materials the actual crack tip is hard to detect. The cracked surfaces are close together, which enhances friction effects behind the crack tip. Therefore special attention has to be given to measuring crack lengths and crack elongation during and after the pre-cracking process.

Three methods were used:

(a) Side-light technique (Fig. 2). The crack lengths were measured after pre-cracking and unloading in a microscope on both polished sides of the specimen.

(b) Post-test investigation (Fig. 3). After the fast fracture test the cracked surfaces were investigated. A transition from inter-granular to trans-granular fracture was detected which separates the precracking region from the load-controlled, fast-fracture toughness test region. The pre-crack front was always found to be straight.

(c) Direct, visual observation (Fig. 4). The pre-cracking process was directly observed with a travelling microscope at a magnification of × 250 [7]. With direct observation the crack length could be measured while the specimen was under load. This method facilitates detection of the crack tip. The kinetics of crack growth, secondary crack formation, crack branching and microcracking may also be observed using this technique.

The specimens were polished but not etched, as the width of the grain boundaries is of the same dimension as the distance of the cracked surfaces near the crack tip. Table I shows crack length values for two examples, measured using the three different methods. There is no significant difference between the results of the three evaluation methods. The mean scatter in crack length was found to be about 3%.

### 2.3. The crack resistance curve

The pre-cracked specimens were rapidly loaded to fracture in a load-controlled test at a loading rate of 100 N sec$^{-1}$. Thus subcritical crack extension was avoided and a true critical test was performed. The fracture toughness $K_{Ic}$ was then calculated using the linear elastic equation

$$K_{Ic} = \tfrac{1}{2}\frac{P_c S}{BW^{1.5}}\,a_c^{1.5}\,Y(a/W) \qquad (1)$$

where $P_c$ = critical load, $S$ = span, $B$ = specimen thickness, $W$ = specimen width, $a_c$ = critical total crack length (notch length + sharp crack length), $Y(a/W)$ = correction function [8].

The $K_{Ic}$ data are plotted against the total normalized crack lengths $a/W$, producing the $K_R$ curve. Equation 1 implies that the cracked surfaces are stress-free or traction-free, where $a_c$ is the crack length measured. Equation 1 does not account for friction effects and adhesive forces behind the measured crack tip. Traction-free surfaces are certainly guaranteed if narrow notches instead of sharp, natural cracks are used.

## 3. Materials

Four alumina materials of different grain size and purity were used. Three were commercially pure; the fourth, $Al_2O_3$–S, was of a debased quality with a glassy phase content of about 3 wt % $SiO_2$ (Table II).

It is well known that the internal stresses of alumina materials increase with increasing grain size. Therefore microcracking and secondary crack formation, and thus the capability for energy dissipation

*Figure 2* Crack length measurement by side-light technique.

*Present address*: Max-Planck-Institute für Metallforschung, Seestrasse 92, 7000 Stuttgart 1, Federal Republic of Germany.

0022–2461/86 $03.00 + .12 © 1986 Chapman and Hall Ltd.

TABLE I Comparison of crack length measurements

| Examples for scatter | Crack length (mm) | | | |
|---|---|---|---|---|
| | Direct observation | Side-light technique | Fracture surface observation | Mean value |
| Mean (Specimen 361) | 2.282 | 2.432 | 2.398 | 2.371 ± 3.3% |
| Maximum (Specimen 571) | 2.367 | 2.688<br>2.528 | 2.807<br>2.749 | 2.626 ± 6.8% |

TABLE II Properties of materials

| Material | Composition (wt %) | Grain size (μm) | Young's modulus, 20° (GPa) | Density (kg m$^{-3}$) |
|---|---|---|---|---|
| $Al_2O_3$ | 97% $Al_2O_3$ + 3% $SiO_2$ | 9 to 11 | 360 | 3.82 |
| $Al_2O_3$-fg | 99.7% $Al_2O_3$ + 0.3% MgO | 1 | 378 | 3.94 |
| $Al_2O_3$-bio | 99.8% $Al_2O_3$ + 0.2% MgO | 3 | 391 | 3.95 |
| $Al_2O_3$-Al 23 | 99.6% $Al_2O_3$ + 0.4% MgO | 20 to 40 | 350 | 3.87 |
| $ZrO_2$-PSZ | Ca + MgO stabilized, 10 vol % tetragonal | 60 | 210 | 5.75 |

should be enhanced with larger grains. In this sense $Al_2O_3$-Al 23 has a greater capability for microcrack formation than (e.g.) $Al_2O_3$-fg.

The glassy-phase material is thought to have less tendency to crack branching, as the second phase and the comparatively smaller grains prevent high internal stresses.

The partially stabilized zirconia $ZrO_2$-PSZ contains about 10 vol % tetragonal phase, which is transformed to monoclinic phase when the crack elongates (stress-induced transformation [9]). This zirconia material has large grains of nearly 60 μm diameter and has been found to be susceptible to crack branching [10]. Furthermore, the volume change after transformation should induce compression forces at the cracked surfaces. In a subcritical displacement-controlled test the material exhibits non-linear stress–strain behaviour [10], which is similar to the behaviour of coarse-grained alumina.

## 4. Results

The $K_R$ curve ($K_{IC}$ against $a/W$) referring to a more fine-grained alumina material $Al_2O_3$–bio (Table I), Fig. 5, shows a linear dependency on measured fracture toughness as a function of normalized crack length $a/W$. The straight line, obtained by regression, remains nearly horizontal at a slope of 0.13. The mean fracture toughness of $K_{IC} = 4.1 \pm 0.8\,MPa\,m^{1/2}$ is in good agreement with values obtained using narrow notches (notch root radius $\varrho \leq 60\,\mu m$) where the surfaces are completely traction-free [11].

The regression line of $Al_2O_3$–fg (Fig. 6) shows a slope of only 0.68. The crack resistance curve may therefore be considered flat. On omitting the fracture toughness data for $a/W > 0.9$ the slope is even lowered to 0.34. As the correction function rises steeply to infinity if $a/W$ approaches unity, small errors in crack length measurement lead to large errors in $K_{IC}$ for $a/W > 0.9$. This explains the large scatter at high $a/W$ values. For illustration, error bars and the $Y$ function are drawn in Fig. 6. The mean $K_{IC}$ value of $4.5 \pm 0.5\,MPa\,m^{1/2}$ is in good agreement with data obtained using narrow notches (Fig. 6), shown by open symbols; in all the diagrams the error bars for the $K_{IC}$ measurements with notched specimens are of the size of the diameter of the symbols.

In contrast with the results above for comparatively fine-grained alumina materials, a steeply rising $K_R$ curve was measured for the coarse-grained $Al_2O_3$–Al 23 (Fig. 7). The results correspond to pronounced non-linear stress–strain behaviour during the subcritical precracking process. Using the traction-free linear-elastic Equation 1, the fracture toughness value increases from $K_{IC} = 2.3\,MPa\,m^{1/2}$ at $a/W = 0.3$ (which is low) up to $10\,MPa\,m^{1/2}$ at $a/W = 0.9$, which is extremely high for alumina materials.

The broken line in Fig. 7 compares the results of a subcritical displacement-controlled test (displacement rate $3\,\mu m\,min^{-1}$) [12] with those of the critical test procedure used in Fig. 7 (closed symbols). Obviously the quality of a steeply rising crack resistance curve remains the same. The data for the critical test are usually located beneath the subcritical ones, indicating an effect of loading rate and different activating processes depending on the test procedure. For the present case the curves seem to be identical.

Notching the $Al_2O_3$–Al 23 specimens results in a completely flat $K_R$ curve (open symbols in Fig. 7). This gives a strong indication that the steep rise of the $K_R$ curve may be due to friction effects behind the actual crack front. The mean traction-free $K_{IC}$ value of notched specimens was about $3\,MPa\,m^{1/2}$, which is somewhat lower than the data for the fine-grained alumina materials.

The $K_R$ curve of the debased alumina $Al_2O_3$–S is given in Fig. 8. The slope of the regression line is only 0.61. This $K_R$ curve may also be considered flat. The mean fracture toughness scatters about $3\,MPa\,m^{1/2}$ and exhibits (somewhat) lower values than that measured with narrow notches. Obviously the $Al_2O_3$–S is more notch-sensitive than the commercially pure materials, and the notch root radius used ($\varrho \leq 60\,\mu m$) may be somewhat too large to simulate natural sharp cracks [13].

The crack resistance behaviour of the PSZ material is shown in Fig. 9. The curve remains completely flat, though crack branching (distinct single long cracks) was found [10] (Fig. 10). The mean fracture toughness of the pre-cracked specimens was $4.8\,MPa\,m^{1/2}$, which is nearly identical to data measured from notched ones ($4.9 \pm 0.1\,MPa\,m^{1/2}$). The results are surprising, as crack branching and transformation-induced internal stresses should result in friction effects and energy dissipation processes, so that behaviour similar to $Al_2O_3$–Al 23 would be anticipated.

## 5. Discussion

It is obvious from the results above that the existence or non-existence of a rising crack resistance curve measured in a critical test procedure depends on the type of microstructural features present. Increasing the grain size in alumina materials increases the internal stresses and the potential for microcracking and secondary crack formation. This may lead to a higher degree of energy dissipation. Damage during crack growth was therefore found especially in the coarse-grained $Al_2O_3$–Al 23 material. This behaviour prompted a more detailed post-test fracture surface investigation.

Fig. 11 shows the fracture surfaces of the $Al_2O_3$–bio material which has a fine-grained microstructure. Fig. 11a shows the area of slow crack growth (pre-cracking process), Fig. 11b the area near to the crack tip and

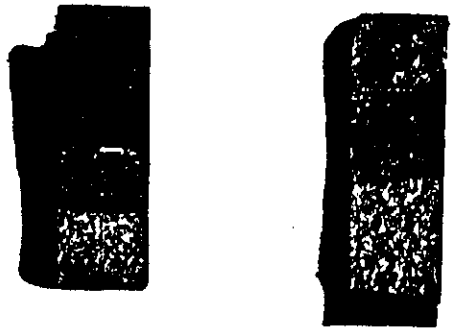

*Figure 3* Transition from inter-granular to trans-granular fracture surface appearance.

*Figure 4* Crack length measurement by direct visual observation and photography.

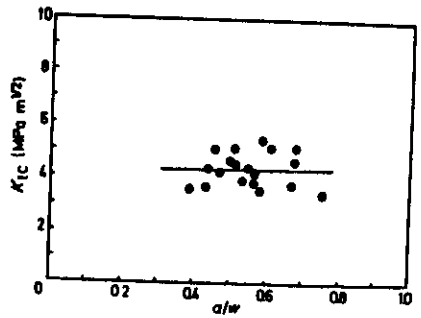


*Figure 5* $K_R$ curve for fine-grained pure alumina $Al_2O_3$–bio: sharp pre-cracking and fast fracture in air at room temperature (20°C). The straight line has a slope of 0.13.

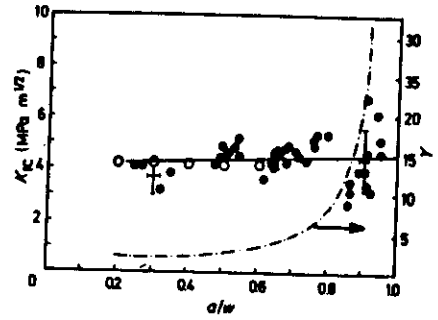


*Figure 6* $K_R$ curves for fine-grained alumina $Al_2O_3$–fg: sharp pre-cracking and fast fracture of pre-cracked and notched specimens in air at room temperature (20°C). (●) pre-cracked, (○) notched specimens; (—) $K_R$ for slope 0.34; (— · —) correction function $Y$

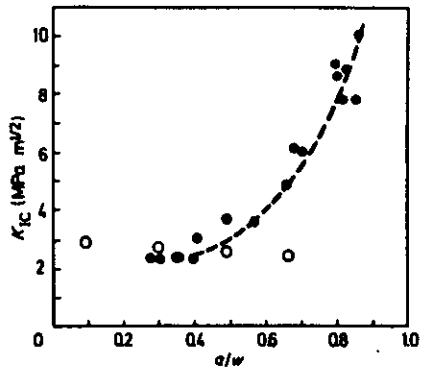


*Figure 7* $K_R$ curves for coarse-grained alumina $Al_2O_3$-Al 23 in air at room temperature (20 °C): sharp pre-cracking and fast fracture of pre-cracked and notched specimens, and for comparison sharp cracking and displacement-controlled loading [12]. (●) $K_R$, critical test; (○) $K_R$, notched specimen; (— — —) $K_R$, subcritical test.

Fig. 11c the area of fast crack growth in a $K_{IC}$ test. A more intergranular fracture surface appearance is found for the lower crack velocity (pre-cracking), whereas the fracture seems to be more transgranular at high crack velocities. A distinct transition region is obvserved (Fig. 11b).

In contrast the fracture surfaces of $Al_2O_3$–Al 23 (Fig. 12a, area of slow crack growth; Fig. 12b, area of fast crack growth) look crushed and split. These phenomena are confirmed by observations of the crack path on the polished specimen surfaces [12] (Fig. 13).

It is important to note that some kind of "process zone" developing at the measured crack tip, which could explain the rising crack resistance curve, was not detected. It is much more likely that the damaged material behind the actual crack tip causes friction effects which, with increasing crack length, may increase and dissipate energy.

The traction-free relation of Equation 1 is no longer suitable, if friction effects or adhesive forces are act-

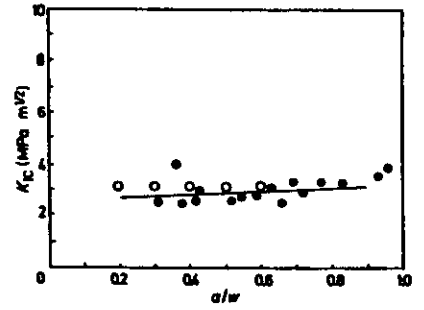


*Figure 8* $K_R$ curves for debased alumina $Al_2O_3$–S: sharp pre-cracking and fast fracture of pre- cracked and notched specimens in air at room temperature (20° C). (●) $K_R$; (—) $K_R$, slope 0.61; (○) $K_{IC}$, notched specimen.

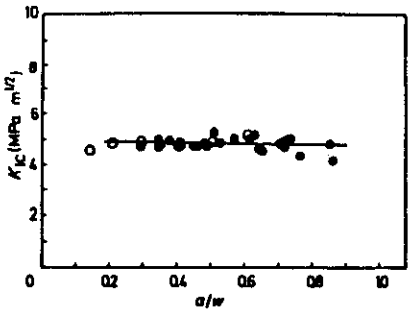


*Figure 9* $K_R$ curves for partially stabilized zirconia $ZrO_2$–PSZ: sharp pre-cracking and fast fracture of pre-cracked and notched specimens in air at room temperature (20° C). (●) $K_R$; (—) $K_R$, slope 0.13; (●) $K_{IC}$, notched specimen.

ing. It may simply and formally be replaced, using a procedure well established for metallic materials, by an expression for an effective stress intensity $K_{IC\,eff}$ defined with an effective crack length $a_{eff}$ [15]:

$$\left.\begin{aligned} a_{eff} &= a_0 + d \\ K_{IC\,eff} &= \sigma_c a_{eff}^{1/2} Y \end{aligned}\right\} \qquad (2)$$

where $a_0$ is the measured critical crack length and $d$ the characteristic size of a friction zone behind the measured crack front, which in this case has to be subtracted and may increase with increasing sharp crack length.

It should be mentioned that in cases where crack branching and secondary crack formation occur, and in cases where the actual crack tip is hard to detect (there is no macroscopic crack tip blunting), defining and measuring an effective crack length will be difficult but decisive.

Nevertheless, displacement-controlled experiments with direct observation and measurement of crack extension allowed for a first rough evaluation of the size of this friction zone [7, 16].

For the measurements above it can be unambiguously stated that fine-grained alumina materials have flat $K_R$ curves which are attributable to stress-free fracture surfaces. Materials with larger grains promote microcracking and crack branching, causing friction effects behind the crack front which result in a rising $K_R$ curve if Equation 1 is used.

Referring to the literature [6, 10] and to Fig. 10, a rising $K_R$ curve is also to be expected for the PSZ material. As visible from the fracture surfaces (Fig. 14), crack branching in the slow crack-growth area is apparent. It was surprising therefore that the $K_R$ curve remained completely flat.

There are indications that for the PSZ material crack branching in the form of isolated large cracks exists, rather than a completely crushed region [10]. Perhaps this behaviour is influenced by a glassy phase at the grain boundaries. It may then be assumed that the fast-fracture test activates only the most dangerous flaw and diminishes the capability for energy dissipation.


*Figure 10* Crack-branching in zirconia $ZrO_2$-PSZ at room temperature [14].

Finally, for the debased alumina material $Al_2O_3$–S the completely flat $K_R$ curve and the lack of any crack branching is mostly attributable to the glassy phase at grain boundaries, which is thought to reduce internal stresses during fabrication.

## 6. Summary and conclusion

$K_R$ curves measured in a load-controlled critical fracture test with ceramic materials are normally horizontal. The $K_{IC}$ data are practically identical with those measured with narrow notches. The fracture surfaces may therefore be assumed traction-free as is the case with notches, and Equation 1 may be used.

Amongst the five materials tested a coarse-grained alumina constituted an exception. It is assumed that in this material high internal stresses lead to enhanced microcracking and overall damage of the microstructure. A process or microcracking zone in front of the actual crack tip could not be detected. The energy dissipation processes could be confined mostly to a zone of destruction $d$ behind the actual crack tip. This zone enlarges with increasing crack length. In this case a rising crack resistance cruve is measured independent of the experimental procedure of loading, whether subcritical displacement-controlled or critical load-controlled. If crack branching and secondary crack formation occur it is difficult to define a crack length. It is thought that this may be one of the main obstacles to obtaining reliable fracture toughness values.

The PSZ material, which also shows crack branching during the precracking process, has a completely flat $K_R$ curve. It is thought (as the overall damage to the microstructure is much less than for the

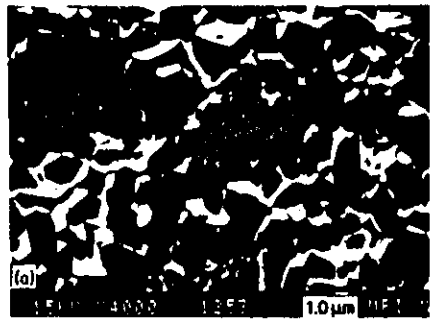


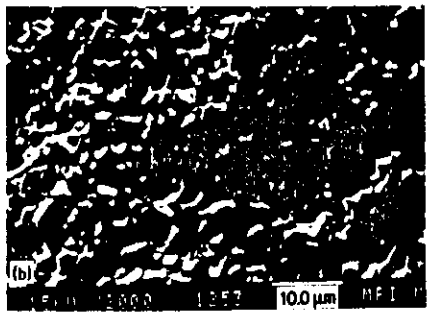


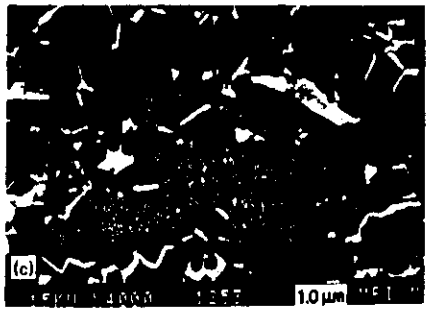


*Figure 11* Fracture surface appearance of alumina $Al_2O_3$–bio: (a) area of slow crack growth, (b) transition region at crack front, (c) area of fast crack growth.

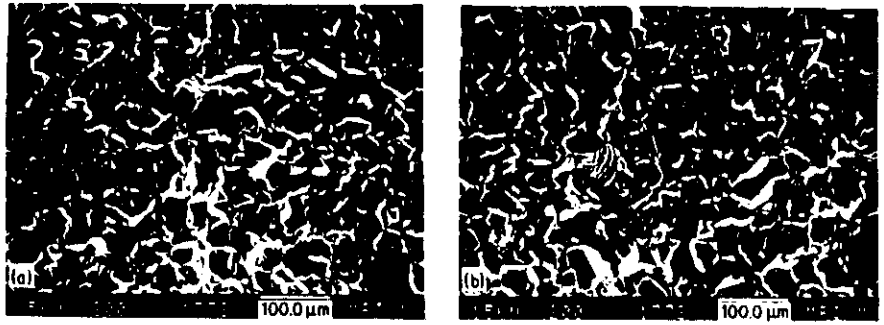


*Figure 12* Fracture surface apppearance of alumina $Al_2O_3$–Al 23: (a) area of slow crack growth, (b) area of fast crack growth.

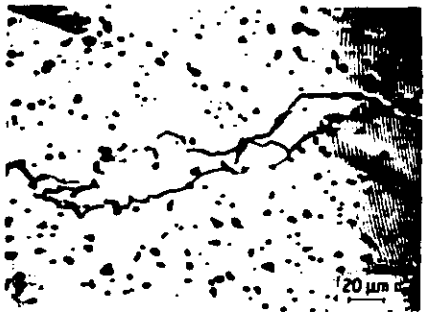


*Figure 13* Crack path on the surface of $Al_2O_3$–Al 23 [12].

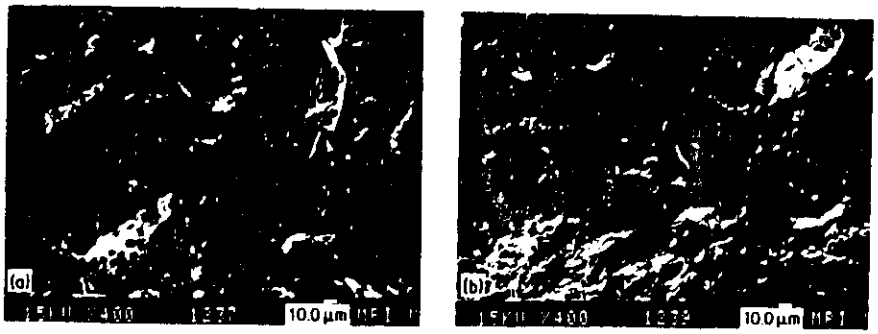


*Figure 14* Fracture surface appearance of zirconia $ZrO_2$–PSZ: (a) area of slow crack growth, (b) area of fast crack growth.

coarse-grained alumina) that in a critical test only the most dangerous flaw is activated.

## References


1. R. F. PABST, J. STEEB and N. CLAUSSEN "Fracture Mechanics of Ceramics," Vol. 4 edited by R. C. Bradt, D. P. H. Hasselman, and F. F. Lange (Plenum Press, New York, 1978) p. 821.
2. U. KROHN, PhD thesis, University of Stuttgart (1979).
3. F. W. KLEINLEIN, *Fortschr. Ber. (Verein Deutscher Ingenieure – Zeitschrift)* 18 (1980) 33.
4. Z. HUEBNER and W. JILECK, *J. Mater. Sci* 12 (1977) 117.
5. R. STEINBRECH, R. KNEHANS and W. SCHAARWÄCHTER, *ibid.* 18 (1983) 265.
6. R. H. J. HANNINK and M. U. SWAIN, *J. Aust. Ceram. Soc.* 18 (1982) 53.
7. A. C. BORNHAUSER, K. KROMP and R. F. PABST, *J. Mater. Sci.* 20 (1985) 2586.
8. J. E. SRAWLEY, *Int. J. Fract.* 12 (1976) 475.
9. LI SHING LI and R. F. PABST, *J. Mater. Sci.* 15 (1980) 2861.
10. W. VOGEL and R. F. PABST, Proceedings of 2nd International Conference on Creep and Fracture of Engineering Materials and Structures, Pineridge, Swansea, England, 1984, Part I, p. 485.
11. A. C. BORNHAUSER, Master thesis, University of Vienna (1980).
12. T. HAUG, private communication (1983).
13. R. F. PABST, "Fracture mechanics of Ceramics," Vol. 2, edited by R. C. Bradt, D. P. H. Hasselman and F. F. Lange (Plenum, New York, 1978) p. 555.
14. W. VOGEL, private communication (1983).
15. D. S. DUGDALE, *J. Mech. Phys. Solids* 18 (1960) 100.
16. T. HAUG, PhD thesis, University of Stuttgart (1985).


*Received 5 October 1984*
*and accepted 25 February 1985*

JOURNAL OF MATERIALS SCIENCE 22 (1987) 1352–1358

# Crack resistance curves of alumina at high temperatures

H. WIENINGER, K. KROMP*
*Institut für Festkörperphysik, University of Vienna, A-1090 Vienna, Austria*
R. F. PABST†
*I.S.M.R.A. U.A.251 Université de Caen, France*

Ceramic three-point bend specimens were pre-cracked in a displacement-controlled test in air at room temperature to form sharp cracks of different lengths. Critical stress intensity factors ($K_{IC}$) were then measured as a function of sharp crack length in a fast-fracture, load-controlled test at 900, 1000 and 1100° C. By means of these fast fracture tests, crack resistance curves ($K_{IC}$ against crack length) were determined for two commercially pure aluminas of different grain size and for a debased alumina containing a glassy phase. The crack resistance curve for the pure, fine grained alumina proved to be flat at 900° C, as was found for room temperature. A steeply rising crack resistance was, however, observed for the pure coarse-grained alumina at 1100° C and for the debased alumina at 1000 and 1100° C. This rise in $K_R$ curves is explained by friction effects of the cracked microstructure behind the crack front for the coarse grained alumina and by adhesive forces caused by the second phase behind the crack front for the debased alumina. These facts are proved by comparison to experiments on notched specimen and by annealing experiments. From the annealing experiments the size of the adhesive zone is estimated for the debased material.

## 1. Introduction

The brittleness of ceramics implies that the crack resistance $R$ should be independent of crack length and that the fracture toughness is seen as a single parameter independent of specimen dimensions and experimental procedure. This is different from metallic materials, where it is well known that the crack resistance may depend strongly on crack length. This fact is attributed to an increasing size of a plastic zone at the tip of the crack under plane stress conditions, accompanied by macroscopic blunting at the onset of crack extension. A plastic zone of comparable size cannot be found in brittle ceramic microstructures and therefore the condition for the existence of a fracture toughness parameter (materials constant) as a function of yield stress, plastic zone size radius and specimen dimensions are not fulfilled.

It is therefore most surprising that, similar to metallic materials, a dependence of crack resistance (fracture toughness) on crack length has been found [1]. It is significant in that context that the phenomenon was observed only in the case where sharp natural cracks instead of narrow notches were introduced as crack starters. It could be proved [1, 2] that crack resistance curves evaluated with different notch depths behave completely flatly. In addition a paradoxon was detected [1] in so far as fracture toughness values measured using narrow notches were equal to or smaller than those found for sharp cracks. According to notch-stress concentration factor analysis the opposite has to be anticipated. Based on these first results a discussion has been developed about the reasons and the importance of raising crack resistance curves in ceramic materials.

## 2. First results and explanations

In an analogy to plasticity reactions the effect is explained by a "process zone" seen as a region of microcrack formation *ahead* of the crack tip [3]. The rising crack resistance is explained by a magnification of that "zone" with increasing crack length. Yet, a "process zone" necessary to explain the distinct increase of fracture toughness could not be detected. It was argued, therefore, [2, 4], that friction effects or adhesive forces *behind* the actual crack tip are more likely to be responsible for the effect. These arguments were supported by measurements with narrow notches which guarantee traction-free surfaces. Traction-free surfaces are also found with metallic materials at the onset of crack extension if macroscopic blunting occurs, thus simulating a narrow notch. Nevertheless, an increase of crack resistance is found due to plastic zone extension. As macroscopic blunting does not occur in ceramic materials, the cracked surfaces keep close together, which allows friction and adhesive forces to act even under load. One could then easily imagine that a "zone" of friction and adhesion *behind* the actual crack tip is enlarged as the crack extends. Phenomenologically this is very similar to the magnification of a plastic or "process zone" in front of a crack. The "zone" behind the crack reaches its final length if the crack opening, a certain distance behind the actual crack tip, becomes so large that the contact between the cracked surfaces is lost. It is easily realized that the length or rather the "effectiveness" of the "zone" behind the crack tip depends on

(a) microstructure and composition
(b) temperature
(c) test procedure (load controlled, displacement controlled, loading rate)
(d) crack velocity
(e) time (oxidation, annealing, transformation reactions).

In particular if at elevated temperatures viscous second phases act as a binder between the cracked surfaces, the temperature and the test procedure play a dominant role. Therefore it should be emphasized that to characterize the quality of the crack resistance behaviour, well defined experimental parameters thus are necessary. This is also a prior condition for comparing any results. Therefore, in this paper catastrophic failure is based on rapid loading conditions in a load controlled test, avoiding subcritical crack extension prior to critical failure. Other and forthcoming papers deal with subcritical, displacement controlled tests at elevated temperatures [5].

## 3. Materials

For the experiments different qualities of $Al_2O_3$ were used as listed in Table I. Two qualities are commercially pure, $Al_2O_3$-S denotes a debased quality with a certain glassy phase content. In a hexagonal structure internal stresses increase with grain size. Therefore microcracking and friction effects may be increased by increasing the grain size as it was shown in a previous paper referring to room temperature reactions [2]. This is not to be expected with small-grained commercially pure materials.

The glassy-phase material is thought to provoke adhesive effects behind the actual crack tip, which may depend strongly on temperature and loading rate [6, 7].

## 4. Experimental procedure

The experimental procedure includes the following steps:

(i) the precracking process
(ii) the crack length measurement
(iii) $K_R$ curve evaluation
(iv) annealing experiments
(v) investigation of the fracture surface

The annealing experiments were conducted at various temperatures and annealing times to account for the annealing procedure of sharp cracks especially if glassy second-phase reactions take place. The area of annealing at the cracked surfaces was then measured and related to the quality of the $K_R$ curve. Referring to the precracking process three-point bend specimens 7 mm × 2.5 mm × 40 mm in size (span width 30 mm) were notched to a normalized notch depth of 0.2 mm and then precracked in air at room temperature to the desired sharp crack lengths using a completely displacement-controlled test at a displacement rate of only 1 $\mu$m min$^{-1}$. The rate ws directly measured and controlled by a LVDT in contact to the lower specimen surface. The specimens were then unloaded. The crack lengths were measured using a side-light technique on both sides of the specimen. As shown in a previous paper [2] a comparison with (a) post-mortem investigations at the cracked surfaces and (b) direct visual observation of the crack extension gives nearly the same result in crack length. It is important to know, if crack branching occurs, the nature of the kinetics of subcritical crack extension during displacement. This too may be investigated thoroughly by direct visual observation. The measured sharp crack length together with the notch length was then used as the crack length $a$ in the linear elastic equation of the form [8]

$$K_R = \frac{3PS}{2BW^2} a^{1/2} Y(a/W) \quad (1)$$

with

$$Y(a/W) = Y(\alpha) = \frac{1.99 - \alpha(1-\alpha)(2.15 - 3.93\alpha + 2.7\alpha^2)}{(1+2\alpha)(1-\alpha)^{1.5}} \quad (2)$$

where $P$ is the critical load, $S$ the span width, $B$ the specimen thickness, $W$ the specimen width and $Y(a/W)$ the correction function.

The measured apparent critical $K_R$ data were then plotted against the normalized crack lengths $a/W$, giving the $K_R$ curve. The linear elastic relation (1) implies that the cracked surfaces are traction free with the traction free crack length $a$ but it does not account for friction effects, adhesive forces and annealing effects behind the measured crack tip. It also implies linear elastic behaviour in front of the actual (visually observed) crack tip, excluding relaxation processes.

The specimens where heated up to the test temperatures of 800, 900, 1000 and 1100° C within 10 min and cracked in a rapid load controlled test at a loading rate of 1000 N sec$^{-1}$. As it was found that healing

TABLE I Properties of materials

| Material | Composition (wt %) | Grain size ($\mu$m) | Young's modulus, 20° (GPa) | Density (kg m$^{-3}$) |
|---|---|---|---|---|
| $Al_2O_3$ | 97% $Al_2O_3$ + 3% $SiO_2$ | 9 to 11 | 360 | 3.82 |
| $Al_2O_3$-fg | 99.7% $Al_2O_3$ + 0.3% MgO | 1 | 378 | 3.94 |
| $Al_2O_3$-Al23 | 99.6% $Al_2O_3$ + 0.4% MgO | 20 to 40 | 350 | 3.87 |

* *Present address*: Max-Planck-Institut für Metallforschung, Seestraße 92, 7000 Stuttgart 1, Federal Republic of Germany.
† The death of Dr R. F. Pabst is sadly recorded. (On leave of absence from Max-Planck-Institut für Metallforschung, Seestraße 92, 7000 Stuttgart 1, Federal Republic of Germany).

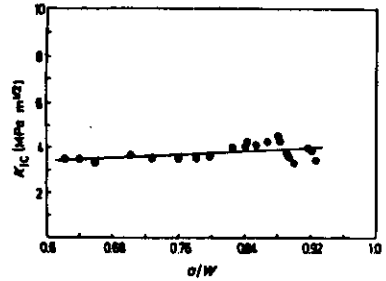

*Figure 1* $K_R$ curve for fine-grained pure alumina $Al_2O_3$-bio: Sharp pre-cracking and fast fracture in air at 900° C. The straight line has a slope of 1.9.

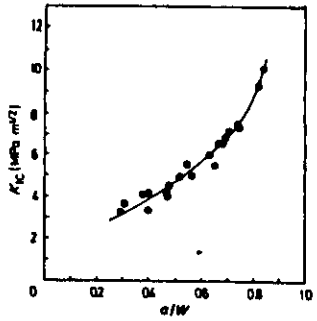

*Figure 2* $K_R$ curve for coarse-grained alumina $Al_2O_3$-A123 in air at 1100° C: Sharp pre-cracking and fast fracture of pre-cracked specimens.

effects are likely to occur due to glassy phase reactions between the cracked surfaces, crack-annealing experiments were performed where the precracked specimens were tempered at 900, 1000 and 1100° C for 10 min, 4 h and 24 h and then fractured at room temperature. The fracture surfaces of the specimens were investigated by SEM.

## 5. Results and discussion

### 5.1. $K_R$ curves as a function of temperature

The high temperature results are given in Figs 1 to 3. For a commercially pure and fine grained material ($Al_2O_3$-fg) a nearly flat $K_R$ curve is measured at 900° C (Fig. 1). This is comparable to room temperature behaviour but with fracture toughness values at a lower level [2]. It is thus possible to define a single fracture toughness parameter at that temperature widely independent of crack length.

In contradiction to the behaviour above the coarse grained material $Al_2O_3$-A123 shows a distinct increase in fracture toughness which corresponds exactly to the room temperature behaviour [2]. Obviously even a test temperature of 1100° C does not change the friction reactions caused by the coarse grained microstructure (Fig. 2).

Compared to room temperature behaviour the $K_R$ curve dependencies change tremendously if a fine-grained material with a second viscous phase is used (material $Al_2O_3$-S). The results are given in Figs 3a, b and c. First it is important to note that the fracture toughness values with notched specimens are completely independent of notch length, as anticipated. This is also the case for sharp cracks at the lower temperature of 900° C. However, increasing the temperature to 1000° C or even 1100° C, results in a steep increase of the $K_R$ curve. The slope of the curve increases with increasing temperature. This steepness in slope is influenced by two effects:

1. the development of a certain region behind the crack front, where the second phase is activated during the time necessary for heating up (10 min)
2. by the level of the test temperature, which influences the dynamic activation of the second phase

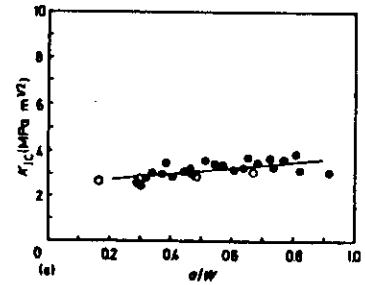

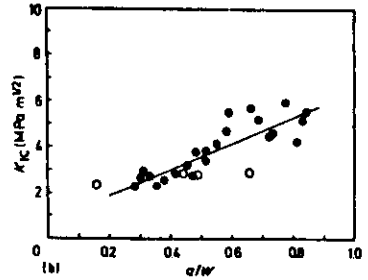

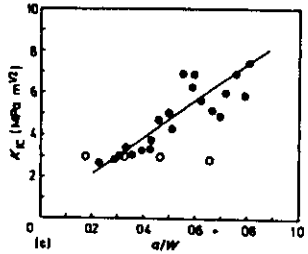

*Figure 3* $K_R$ curves for debased alumina $Al_2O_3$-S: Sharp pre-cracking and fast fracture of pre-cracked and notched specimens in air (●) $K_R$; (——) $K_R$ slope; (○) $K_{IC}$, notched specimen. (a) 900° C; (——) $K_R$, slope 1.25 (b) 1000° C; (——) $K_R$, slope 5.7, (c) 1100° C; (——) $K_R$, slope 8.76.

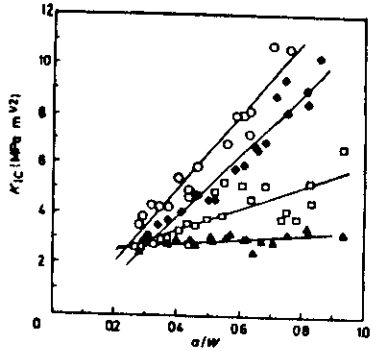

*Figure 4* $K_R$ curves for debased alumina $Al_2O_3$-S: Sharp pre-cracking, annealing at high temperature and fast fracture of pre-cracked specimens in air at room temperature (20° C). (▲) Annealing at 1000° C for 10 min, (□) annealing at 1100° C for 10 min, (◆) annealing at 1000° C for 4 h, (○) annealing at 1100° C for 4 h.

at the crack front during the test procedure at a constant high loading rate.

To investigate these dynamic effects during the test procedure and to give an estimation of the size of the active zone behind the crack front, annealing experiments were performed.

### 5.2. Annealing effects concerning material $Al_2O_3$-S

In the case of the material with the glassy phase a distinct annealing process was detected which depends on the holding time and the annealing temperature. Attention should be paid to the fact that the fracture toughness values were measured after cooling down to room temperature again to estimate the size of the active zone behind the crack front mentioned above.

For a short holding time of 10 min the $K_R$ curve remains flat at an annealing temperature of 1000° C, whereas for 1100° C with this holding time a rising $K_R$ curve is found (Fig. 4). Compared to the test results

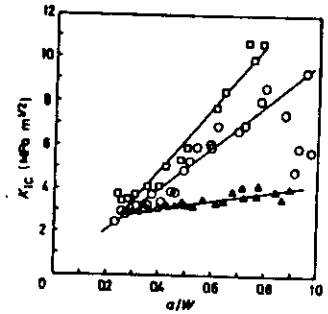

*Figure 5* $K_R$ curves for debased alumina $Al_2O_3$-S: Sharp pre-cracking, annealing at high temperature and fast fracture of pre-cracked specimens in air at room temperature (20° C). (▲) Annealing at 900° C for 24 h, (○) annealing at 1000° C for 24 h, (□) annealing at 1100° C for 24 h.

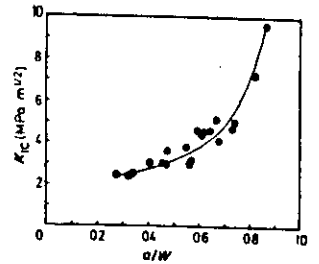

*Figure 6* $K_R$ curve for coarse-grained alumina $Al_2O_3$-A123: Sharp pre-cracking, annealing at 1100° C for 24 h and fast fracture of pre-cracked specimens in air at room temperature (20° C).

from the last section (Figs 3b and c), the steepness is lowered, which indicates that with these room temperature tests only the reduction of the actual crack length by annealing is considered.

For a holding time of 4 h for both the annealing temperatures of 1000 and 1100 C $K_R$ curves are found, rising to a high extent (Fig. 4). The slopes of the $K_R$ curves at these temperatures were found to be similar to the longest performed holding times of 24 h (Fig. 5), whereas the effect of this holding time at 900° C is only small (compare Fig. 5 to 3a). The comparison with the dynamic tests at the elevated temperature exhibits a steeper increase for the case of annealing for 4 and 24 h and subsequent measurement at room temperature. From this it is obvious that the annealing of the sharp cracks and the development of the zone behind the crack front has a greater effect as the dynamic activation of the second phase during the test at elevated temperatures.

From these experiments and a post mortem investigation the size of the adhesive zone behind the crack front was estimated (see later on).

Concerning the course-grained material $Al_2O_3$-A123 with no glassy phase, annealing experiments do not influence the $K_R$ curve behaviour at all. Even an annealing temperature of 1100° C and 24 h holding time do not change the typical fracture toughness dependence measured at room- and elevated temperatures (compare Fig 2 to 6). It may be stated therefore that for annealing processes at temperatures and times used here, distinct reactions are only found if a second phase exists.

### 5.3. Crack length and crack velocity dependencies

As stated in the introduction the crack resistance behaviour additionally may depend on crack velocity and thus on the experimental procedure. This is the main reason to perform a well defined experimental procedure. In addition it was found [9] that the crack velocity in sharp cracked specimens may depend on crack length. Taking account for the results in Fig. 7 the crack velocity at a constant loading rate increases as the crack length decreases. This behaviour is obviously a function of the stored energy which is larger at shorter crack lengths thus resulting in larger initial

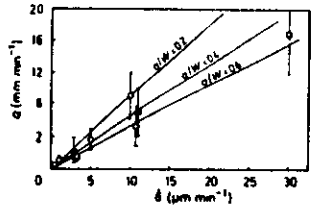


*Figure 7* Dependence of crack velocity for debased alumina $Al_2O_3$-S at 1000 C on loading rate $\dot{\delta}$ for different crack lengths $a/W$.

velocities. This fact leads to lower fracture toughness values for the case of shorter crack lengths due to embrittlement reactions of the glassy phase at these high initial velocities. For this, even at a high constant loading rate in a load controlled test the rising $K_R$ curve may at least partly be explained by embrittlement reactions due to different initial velocities.

Furthermore, if subcritical crack extension takes place before catastrophic failure occurs, the error in crack length measurement is comparatively larger with short than with long cracks, leading also to an apparent increase in fracture toughness with longer cracks. Those errors increase with decreasing viscosity at higher temperatures.

Apart from the reactions above which in any case are of a secondary nature, it is obvious that the increase of the measured fracture toughness as a function of crack length, temperature and annealing time must be attributed to adhesive and annealing effects *behind* the actual crack front. In particular if second phases exist, the cracked surfaces are not traction free even at the onset of fast fracture. The adhesive zone behind the actual crack tip increases with increasing crack length and temperature. Using Equation 1 which applies solely to traction-free surfaces, the fracture toughness is always overestimated. The overestimation increases with crack length and temperature. This is clearly revealed by the results evaluated with notched specimens, where stress-free surfaces are guaranteed (Figs 3a, b and c). At a certain load velocity in a load controlled test $K_R$ curves with notched specimens behave flatly, independent of temperature. Therefore the formalism used is exactly appropriate to the narrow notch (notch width $\sim 70\,\mu m$) and not to a sharp natural crack, if adhesive or friction effects exist. Consequently, the difference between the measured notch-fracture toughness and that measured with sharp cracks may give a measure for the "length" or better the "effectiveness" of the adhesive zone $z$ behind the actual crack tip.

If the Griffith formula

$$K_I = \sigma a^{1/2} Y \tag{3}$$

holds (which is not always clear if tractions behind the actual crack tip exist) a $K_{eff}$ may be formulated such that

$$K_{eff} = \sigma a_{eff}^{1/2} Y \tag{4}$$

with

$$a_{eff} = a - z \tag{5}$$

$$z = z(\dot{a}, T, \text{composition})$$

where $a$ is the actual measured crack length and $Y$ the correction function. It is clear that in the case of viscous phases, $z$ depends on the crack velocity $\dot{a}$, the temperature $T$ and the composition.

Referring to the annealing effects in $Al_2O_3$, it may be anticipated that no macroscopic blunting exists, instead the sharp crack is filled with glassy phase, the extent of which depends on annealing temperature and time. The second phase gives a strong bond between the cracked surfaces after cooling down to room temperature. Depending on annealing temperature and annealing time the crack may be annealed to a great extent.

An attempt was made to evaluate the zone size $z$ for the material with the second phase. For this the crack lengths were calculated for the experiments with the sharp natural cracks at 900, 1000 and 1100° C under the assumption that the $K_R$ curves remain flat (compare Figs 3a, b and c). The difference between those crack lengths and the measured natural crack lengths gives a measure for this zone size.

The transformation of the Griffith equation results in a fourth order polynomial because of the correction function $Y$, which was solved for this purpose for relevant solutions in the range $0 < a/W < 1$ by interval-packing:

$$\frac{a}{W} Y^2(a/W) - \frac{4}{9} \frac{K_{IC}^2 B^2 W^3}{P^2 S^2} = 0 \tag{6}$$

where $P$ is the load, $S$ the span, $B$ the depth and $W$ the width.

These calculated zone sizes (mean values) are listed in Table II for $a/W = 0.4$, 0.6 and 0.8 at 1000 and 1100° C. At 900° C the rise in the $K_R$ curve and thus the size of the zone is negligible.

TABLE II Evaluation for zone sizes $z$

| Temperature (°C) | $a/W$ | $a_m$ measured (mm) | $a_c$ calculated (mm) | $\Delta a = z$ (mm) | $\Delta a/a_m$ (%) |
|---|---|---|---|---|---|
| 1000 | 0.4 | 2.8 | 2.48 | 0.32 | 11 |
| 1000 | 0.6 | 4.2 | 3.30 | 0.91 | 21 |
| 1000 | 0.8 | 5.6 | 4.81 | 0.79 | 14 |
| 1100 | 0.4 | 2.8 | 2.29 | 0.51 | 18 |
| 1100 | 0.6 | 4.2 | 2.68 | 1.52 | 36 |
| 1100 | 0.8 | 5.6 | 4.57 | 1.03 | 18 |



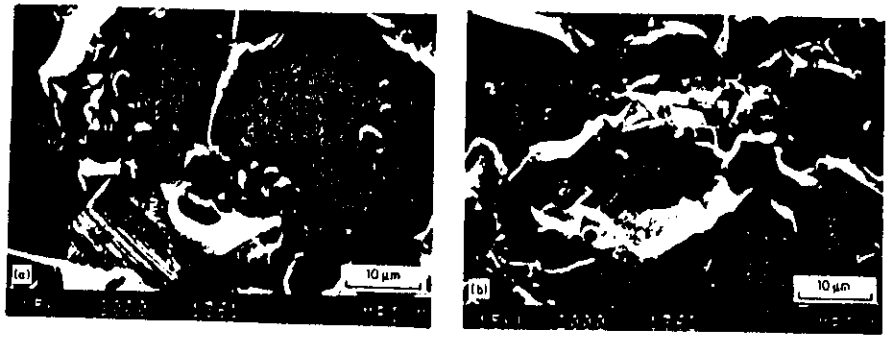


*Figure 8* Fracture surface appearance of debased alumina $Al_2O_3$-S: Sharp pre-cracking, annealing at high temperature and fast fracture of pre-cracked specimens in air at room temperature (20° C). (a) Annealing at 1000° C for 10 min and (b) annealing at 1100° C for 10 min.

For $a/W = 0.4$ and 0.6, the $z$ values show a rising tendency and realistic sizes compared to results from $R$-curve calculations with an energy concept [6]. For $a/W \geqslant 0.8$ the zone size is then obviously reduced again by the, for this case, high crack opening displacement. An investigation of the fracture surfaces in the range of the supposed zones was done by SEM on the specimens broken in the annealing experiments.

For a holding time of 10 min at 1000° C (10 min corresponds to the total holding time for all the high temperature experiments) the glassy phase coates the surface of the grains (Fig. 8a). At 1100° C the second phase concentrates in bands along the edges of the grains (Fig. 8b).

### 5.4. Annealing effects concerning material $Al_2O_3$-Al23

The data evaluated using the coarse grained material correspond well to room temperature measurements. Thus the friction effects behind the actual crack front are independent of temperature and annealing processes. Obviously this commercially pure material is insensitive to everything which does not influence the friction effects caused by the coarse-grained structure. Consequently experiments with notched specimens result in flat $K_R$ curves, as was previously shown at room temperature [2].

### 5.5. High-temperature influence on material $Al_2O_3$-fg

The commercially pure fine grained material should be insensitive to friction effects (small grains, low internal stresses) and also to adhesive forces. Consequently as it is verified at least at 900° C, the $K_R$ curve behaves flatly (Fig. 1).

## 6. Summary and conclusion

The distinct increase of crack resistance measured in a critical load-controlled test as a function of crack length at a distinct high loading rate is similar to that found with metallic materials under plane stress conditions. With metallic materials, however, a plastic zone of increasing size in front of the crack is made responsible for the increase in crack resistance. This is essentially different from reactions in ceramics found in this paper. It is stated that a plastic zone or any other "process zone" of microcracking in front of the crack tip does not exist. Instead, the cracked surfaces keep close together as no macroscopic blunting exists even at the onset of critical fracture. This allows friction and annealing and thus adhesive forces to act *behind* the actual crack tip. The surfaces therefore are not traction-free. A certain zone $z$ of adhesion is formed behind the crack tip. Use of the well known Griffith equation based on traction free surfaces then leads to an apparent increase of fracture resistance. The problem remains in estimating the "length" or better the "effectiveness" of $z$ which depends on microstructure, temperature and loading rate (crack velocity) and time especially if viscous second phases exist. From annealing experiments an attempt was made to evaluate the size of this zone $z$. In the simplest case the Griffith form may be used further with an $a_{eff}$ instead of the actual measured crack length in an analogy to a plastic zone correction used for metallic materials. In any case the much more complex interactions of microstructure, temperature and loading rate in ceramics compared to metallic materials make it understandable that the test procedure itself plays a dominant role. This enlarges appreciably the experimental effects. Also the analytical verification becomes more complex as different ceramic materials behave much more individually at elevated temperatures. Simple analogies to metallic materials are misleading, assuming some sort of "process zone" in front of a crack. This analogy may be useful as a "working hypothesis", but does not account for the real effects which act behind the crack tips and not in front of them.

## References

1. R. F. PABST, J. STEEB and N. CLAUSSEN "Fracture Mechanics of Ceramics", Vol. 4, edited by R. C. Bradt, D. P. H. Hasselman and F. F. Lange (Plenum Press, New York, 1978) p. 821.
2. H. WIENINGER, K. KROMP and R. F. PABST, *J. Mater. Sci.* 21 (1986) 411.
3. F. E. BURESCH, "Advances in Research on the Strength and Fracture of Materials", edited by D. M. R. Taplin, ICF4 Waterloo 1977 (Pergamon Press, New York, 1978) p. 939.

4. R. STEINBRECH, R. KNEHANS and W. SCHAARWÄCHTER, *J. Mater. Sci.* 18 (1983) 265.
5. T. HAUG and R. F. PABST, *J. Amer. Ceram. Soc.*, to be published.
6. A. BORNHAUSER, K. KROMP and R. F. PABST, *J. Mater. Sci.* 20 (1985) 2586.
7. R. F. PABST, K. KROMP, H. WIENINGER, A. BORNHAUSER and T. HAUG, *Fortschr. Ber. Deutsche Ker. Ges.* 1/3 (1985) 5.
8. J. E. SRAWLEY, *Int. J. Fract.* 12 (1976) 475.
9. T. HAUG, PhD thesis, University of Stuttgart (1985).

*Received 30 May*
*and accepted 18 August 1986*